Geobiology

Geobiology (2013), **11**, 570–592 DOI: 10.1111/gbi.12062

Record of archaeal activity at the serpentinite-hosted Lost City Hydrothermal Field

S. MÉHAY,[1,*] G. L. FRÜH-GREEN,[1] S. Q. LANG,[1] S. M. BERNASCONI,[1] W. J. BRAZELTON,[2] M. O. SCHRENK,[2] P. SCHAEFFER[3] AND P. ADAM[3]

[1]*Department of Earth Sciences, ETH Zurich, Zurich, Switzerland*
[2]*Department of Biology, East Carolina University, Greenville, NC, USA*
[3]*Laboratoire de Biogéochimie Moléculaire, Institut de Chimie de Strasbourg UMR 7177, CNRS-Université de Strasbourg, ECPM, Strasbourg, France*

ABSTRACT

Samples of young, outer surfaces of brucite–carbonate deposits from the ultramafic-hosted Lost City hydrothermal field were analyzed for DNA and lipid biomarker distributions and for carbon and hydrogen stable isotope compositions of the lipids. Methane-cycling archaeal communities, notably the Lost City *Methanosarcinales* (*LCMS*) phylotype, are specifically addressed. Lost City is unlike all other hydrothermal systems known to date and is characterized by metal- and CO_2-poor, high pH fluids with high H_2 and CH_4 contents resulting from serpentinization processes at depth. The archaeal fraction of the microbial community varies widely within the Lost City chimneys, from 1–81% and covaries with concentrations of hydrogen within the fluids. Archaeal lipids include isoprenoid glycerol di- and tetraethers and C_{25} and C_{30} isoprenoid hydrocarbons (pentamethylicosane derivatives – PMIs – and squalenoids). In particular, unsaturated PMIs and squalenoids, attributed to the *LCMS* archaea, were identified for the first time in the carbonate deposits at Lost City and probably record processes exclusively occurring at the surface of the chimneys. The carbon isotope compositions of PMIs and squalenoids are remarkably heterogeneous across samples and show highly ^{13}C-enriched signatures reaching $\delta^{13}C$ values of up to +24.6‰. Unlike other environments in which similar structural and isotopic lipid heterogeneity has been observed and attributed to diversity in the archaeal assemblage, the lipids here appear to be synthesized solely by the *LCMS*. Some of the variations in lipid isotope signatures may, in part, be due to unusual isotopic fractionation during biosynthesis under extreme conditions. However, we argue that the diversity in archaeal abundances, lipid structure and carbon isotope composition rather reflects the ability of the *LCMS* archaeal biofilms to adapt to chemical gradients in the hydrothermal chimneys and possibly to perform either methanotrophy or methanogenesis using dissolved inorganic carbon, methane or formate as a function of the prevailing environmental conditions.

Received 22 October 2012; accepted 6 September 2013

Corresponding author: S. Méhay. Tel.: +971 55 900 7865; fax: +971 4 883 54 34;
e-mail: smehay@slb.com

*Present address: Schlumberger, Reservoir Sampling and Analysis, Dubai, UAE

INTRODUCTION

The Lost City hydrothermal field (LCHF), discovered in 2000, is a novel peridotite-hosted hydrothermal system sustained primarily by lithospheric cooling and serpentinization processes (Kelley *et al.*, 2001, 2005; Früh-Green *et al.*, 2003; Allen & Seyfried, 2004). The LCHF is located near the top of the southern Atlantis Massif at 30°N near the Mid-Atlantic Ridge (MAR, Fig. 1) and is underlain by mantle harzburgites that contain > 60% of iron-bearing olivine. Upon contact with seawater, mantle rocks are altered by serpentinization processes (Olivine $((Mg,Fe)_2SiO_4) + H_2O \rightarrow$ Serpentine $(Mg_3Si_2O_5(OH)_4) \pm Fe_3O_4 \pm$ Brucite $(Mg(OH)_2) + H_2$) that produce reducing fluids with high

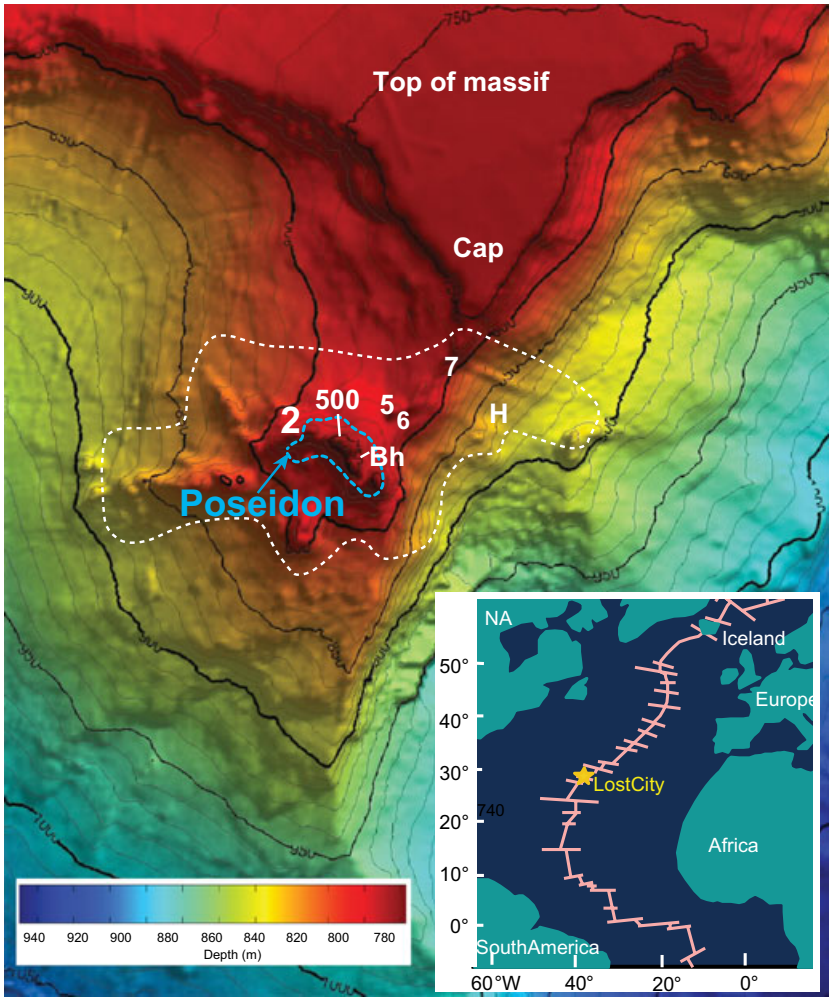

Fig. 1 Bathymetric map of the LCHF as mapped by Autonomous Benthic Explorer and showing vent locations identified by marker numbers. The white dashed line shows the spatial extent of the active field. The internal blue dashed line defines the largest hydrothermal structure Poseidon (60 m high). The LCHF is located on 1–2 million-year-old serpentinized mantle rocks, 15 km west of the axis of the MAR, and hosts numerous active carbonate pinnacles at a water depth of 730–850 m near the summit of the Atlantis Massif.

hydrogen concentrations (e.g., Janecky & Seyfried, 1986; Holm and Charlou, 2001; Früh-Green *et al.*, 2004; McCollom and Bach, 2007).

The LCHF hosts at least 30 active and inactive carbonate–brucite structures. They result from alkaline fluids (pH 10–11) emanating from fault zones that tap the region of active serpentinization in the underlying peridotites (Kelley *et al.*, 2001, 2005; Ludwig *et al.*, 2006). The chimney structures vent warm (28–91 °C) fluids with high concentrations of H_2 (up to 14.4 mmol/kg), CH_4 (1–2 mmol/kg) and formate (36–158 μmol/kg) (Kelley *et al.*, 2005; Proskurowski *et al.*, 2006, 2008; Lang *et al.*, 2010). Radiocarbon dating of carbonate minerals indicates that Lost City has been hydrothermally active for at least 30 000 years (Früh-Green *et al.*, 2003), and more recently, U/Th dating suggests that activity in the area may have been ongoing for >100 000 years (Ludwig *et al.*, 2011).

In the carbonate–brucite towers, the development of ecosystems is most likely limited by the availability and renewal of carbon sources, pH, nutrients, and/or temperature. The dominant carbon species, CH_4, is radiocarbon dead and is mostly produced by subsurface processes related to Fischer–Tropsch- and Sabatier-type reactions from a mantle source of carbon, which implies that a significant amount of abiogenic carbon is transferred from the upper mantle to the biosphere and hydrosphere through serpentinization processes (Proskurowski *et al.*, 2008; Bradley & Summons, 2010). CH_4-metabolizing (producing or consuming CH_4) archaea and methylotrophic bacteria are predominant in the chimneys (Schrenk *et al.*, 2004; Brazelton *et al.*, 2006), suggesting that CH_4 plays an important role in the biogeochemical cycling of carbon in this extreme environment. Dissolved inorganic carbon concentration ($\sum CO_2$ = $CO_{2(aq)}$, HCO_3^-, CO_3^{2-}) is very low in the high pH, anaerobic LCHF chimney fluids (4 μmol/kg on average), and mantle-derived CO_2 is removed in the subsurface through conversion to hydrocarbons or carbonate precipitation (Proskurowski *et al.*, 2008). In addition, other carbon species such as formate and acetate (1–35 μmol/L) are important sources of carbon to sustain microbial activity in this system (Lang *et al.*, 2010, 2012).

The production of H_2, abiotic hydrocarbons, and likely formate during serpentinization reactions and the subsequent mixing of these reduced fluids with oxic seawater provide metabolic energy for chemolithoautotrophic and heterotrophic organisms (McCollom, 2007). Development of an ecosystem depends on the availability and renewal of carbon and nutrient sources, electron donors (such as H_2, CH_4, H_2S, and Fe^{2+}), and electron acceptors (particularly O_2, NO_3^-, and SO_4^{2-}). In ultramafic environments, electron donors are generally unlimited in the form of H_2 and CH_4, whereas electron acceptors will depend greatly on the fate of sulfate, which is 1–4 mM in Lost City fluids (Kelley *et al.*, 2005), as well as seawater recharge and mixing with serpentinizing fluids.

The diversity of archaeal communities is low in the carbonate towers (Schrenk *et al.*, 2004; Brazelton *et al.*, 2010a). In active vents (55–75 °C), ~ 80% of the identified cells within the anoxic interior of the brucite–carbonate chimneys that are in closest contact with vent fluids are archaea and are dominated by a single phylotype of Euryarchaeota referred to as Lost City *Methanosarcinales*, *LCMS* (Schrenk *et al.*, 2004). This new taxon, which is related to both methanogenic and methanotrophic archaea, is found within a biofilm that is tens of micrometers thick and bound to the mineral surfaces (Schrenk *et al.*, 2004; Brazelton *et al.*, 2006). In the exterior parts of the actively venting chimneys that are in closest contact with seawater, the relative abundance of archaea is half that of bacteria, but 50–75% of these archaea belong to the *LCMS* phylotype (Schrenk *et al.*, 2004). In samples collected from inactive (presently non-venting) parts of the hydrothermal structures, where porosity decreases down to 15–30% due to precipitation of calcite from seawater, detectable archaeal cells are again about half as abundant as bacterial cells. In some of these inactive structures, the anaerobic methanotroph ANME-1 dominates (Brazelton *et al.*, 2006). Additional archaeal species found at Lost City include *Thermococcales* (Euryarchaeota) and *Crenarchaeota*, which have been identified in the vent fluids and likely reflect hyperthermophiles thriving in the subsurface basement (Brazelton *et al.*, 2006, 2010a), although some *Crenarchaeota* may represent a pelagic contribution (Schrenk *et al.*, 2004).

Because seawater bicarbonate and mantle-derived abiogenic carbon have distinct radiocarbon signatures, Lang *et al.* (2012) measured the radiocarbon content of bulk chimney biomass to investigate what carbon sources are assimilated by the microbial communities at Lost City. This study identified regional variations and demonstrated that mantle carbon contributes only ~ 10% of the biomass in actively venting carbonate chimneys with the highest temperatures, highest concentrations of H_2 and SO_4^{2-}, and lowest concentrations of HS^-. In contrast, in locations where fluids contain lower concentrations of H_2 and SO_4^{2-}, and higher concentrations of HS^-, consistent with microbial sulfate reduction, up to 50% of the chimney biomass is synthesized from mantle carbon. The chimneys that hosted these low-H_2 and low-SO_4 fluids also had higher amounts of biomass than the higher-temperature chimneys where less mantle carbon was incorporated. This difference was attributed to greater incorporation of mantle-derived, abiogenic methane or formate by the dominant *LCMS* microbial species in locations where sulfate reducers are able to facilitate this assimilation. However, it remains uncertain as to what controls the ability of the microbial communities to utilize the abundant chemical energy in this system and whether the uptake of mantle carbon (e.g., as methane or formate) vs. seawater DIC is preferential to specific groups of bacteria or archaea.

Archaeal membranes show a great structural variety, recorded in lipid biomarkers, which is thought to reflect adaptation to physiological and evolutionary environmental conditions, such as pH (Macalady *et al.*, 2004; Pearson *et al.*, 2008) and temperature (Gliozzi *et al.*, 1983; Uda *et al.*, 2001). Distribution of archaeal lipids might also depend on nutrient availability, source of energy, or level of oxygen (De Rosa & Gambacorta, 1988). Lipid biomarkers in CH_4-metabolizing archaea mainly include C_{25} and C_{30} isoprenoid hydrocarbons as well as glycerol di- and tetraethers with C_{20} or C_{40} isoprenoid and hydroxylated isoprenoid moieties (e.g., Stadniskaia *et al.*, 2003; Stadnitskaia *et al.*, 2008). Here, we focus on archaeal biomarkers from young carbonate–brucite deposits that were collected in 2003 and 2005 at various actively venting sites across the LCHF (Table 1, Fig. 1). The 2005 samples were collected from the surface of the deposits and hence are expected to record interface processes between hydrothermal fluids and seawater in the outer part of the chimneys. Our goal is to use molecular biomarker distributions and compound-specific carbon isotopes in association with genetic data to better understand archaeal activity at the surface of the Lost City carbonate chimneys, whereas the previous study on the molecular biomarker distributions at the LCHF focused on whole pieces of carbonate towers that are expected to reflect mainly the microbial activity in the interior part of the carbonate chimneys (Bradley *et al.*, 2009a). Given the high heterogeneity of the LCHF system, specific and different biochemical processes may exist at the surface of the carbonate chimneys where the temperature and chemical gradients are the highest and lead to adapted microbial carbon assimilation pathways that remain to be elucidated in this extreme environment.

MATERIALS AND METHODS

Field relations and samples

We analyzed samples representative of eight of the main active vents across the field (Table 1, Fig. 1), which were

Table 1 Name, location, and main features of the studied samples and of the associated vent fluids

Sample	Dive name	Location	Depth (m)	Year collected	Venting temp. (°C)*	EM pH‡	EM H_2 (mmol/kg)§	$\delta^{13}C$ (‰) bulk C_{org}
LC-Bh	H06_073005_Bio2slurpA2_0326	Bh	746	2005	91	10.7	9.1	−8.3
LC-500	H03_072705_Bio1slurpA2_0442	Mkr 500 Poseidon (formerly Mkr 3)	732	2005	88	10.5	12.3	−11.2
Chimneys next to Poseidon (north face)								
LC-2a	H05_072905_Bio1slurpA2_0111	Mkr 2 (IMAX flange)	764	2005	71	10.5	3.7	−6.2
LC-2b	H05_072905_Bio2slurpA1_0118	Mkr 2 (IMAX flange)	764	2005	71	10.5	3.7	−15.2
LC-6	H07_073105_Bio2slurpA1_1035	Mkr 6	777	2005	44	9.7	14	−4.16; −1.8
LC-5	H08_080105_Bio5slurpB1_0428	Razorback, near Mkr 5	767	2005	n.d.	n.d.	n.d.	−14.6
Sites further away (north-east from Poseidon), within the active field								
LC-7a	H02_072605_Bio1slurpA2_0354	Mkr 7	802	2005	(51)†	10.4	5.5	−14.5
LC-7b	3867-1228	Mkr 7, 315 ± 12 years old¶	801	2003	(51)†	10.4	5.5	−4.9
LC-Ha	H04_072805_Bio4slu rpA2_0514	Mkr H**	843	2005	64	10.7	1.3	−13.3
LC-Hb	H06_073005_Bio1slurpA1_0142	Mkr H**	843	2005	13	10.7	1.3	−12.4
LC-Hc	3881-1228	Mkr H, 48 ± 3 years old¶**	845	2003	(55)†	10.7	1.3	−13.5
Outside the active field								
LC-Cap	H08_073105_Bio1slurpA1_2109	Cap	742	2005	n.d.	n.d.	n.d.	−11.6

n.d., not determined.*Temperature measured at the time of sampling. Background temperature: 9.8 °C, pH 7.8. †Temperature not determined during sampling. Temperatures in parentheses are maximum *T* measured in 2003. ‡Endmember (EM) pH at 22°C; calculated from linear regression, including an average seawater endmembers, as reported in Lang *et al.* (2012). §Average of all reported values of fluids sampled in 2003, as reported in Proskurowski *et al.* (2008) (see also Lang *et al.*, 2012). ¶Ludwig *et al.* (2011). **Marker H structure is also referred to as the Nature's pinnacle in other studies.

obtained during expeditions in 2003 (R/V Atlantis cruise AT-7-41) and 2005 (National Oceanic and Atmospheric Administration (NOAA) Ocean Explorer cruise). The sites are denoted by field markers left at the hydrothermal structures during expeditions in 2000 (R/V Atlantis cruise AT-3-60) and 2003. The largest of the hydrothermal edifices, Poseidon, is 60 m in height and hosts multiple vents that expel fluids with varying temperatures, pH, hydrogen, and sulfate concentrations. At its summit, fluids are venting on average at 81 °C with a pH of 10.5 (Marker (Mkr) 500 = Mkr 3 in other studies). A small chimney, the so-called beehive structure growing on the north side of Poseidon, is vigorously venting the highest-temperature fluids measured at Lost City (91 °C) and has an average pH of 10.7. The beehive structure had a ~ 1 m new growth as sampling in 2003 provided us a precise time constraint of two years for the corresponding sample analyzed in this study (Lost City Beehive, LC-Bh). The carbonate–brucite structures also include overhanging growths, known as flanges, on the sides of the active chimneys, which tend to pool hydrothermal fluids (e.g., Mkr 2, also referred to as the IMAX flange). Next to Poseidon and northward, smaller carbonate–brucite towers (Mkr 5 and 6) are actively venting. The fluids at the Marker 6 vent site are the highest in hydrogen concentration, with an average endmember concentration of 14 mmol/kg. More distant, actively venting sites are found to the east of the main vent field, and samples were taken at the Mkr 7 and Mkr H (also referred to as Nature Towers) structures. The Mkr H vents are on a ~ 30 m high, multispired structure located directly on the serpentinite basement and emit fluids at temperatures up to 64 °C. The Mkr 7 structure is also characterized by lower-temperature fluids venting at ~ 50 °C. A flat-lying sequence of variably lithified pelagic carbonate ooze and sedimentary breccias forms a sedimentary cap at the top of the Atlantis Massif. The sample denoted with 'cap' refers to a sample taken north of Poseidon from an up to 30-cm-thick carbonate vein, which cuts the sedimentary cap rocks and shows diffuse flow and filamentous carbonate growth at the time of sampling.

The youngest structures, which are in contact with diffusely venting fluids, are composed of aragonite and brucite and have a porosity exceeding 40%. The mineralogy and internal porosity of the chimneys evolve with age to less porous and more calcite-rich structures that reflect progressive seawater flowing into the porous edifices (Früh-Green *et al.*, 2003; Ludwig *et al.*, 2006).

This study includes 10 samples obtained in 2005 by means of a suction sampler (colloquially referred to as a slurp sampler), which consists of a tube connected to a pump that collects the carbonate–brucite deposits and microbial biomass directly from a well-defined part of the surface of the structures into separate, closed plexiglass cylinders (maximum four per dive) that were cleaned

between each dive. Samples were obtained with the remotely operated vehicle *Hercules* on board the R/V Ronald H. Brown, and sample names, given in Table 1, were standardized at the time of sampling: the dive number (H0X), date (MMDDYY), type of sample (*R* = 'rock' collected as a grab sample with the Hercules claw; Bioslurp = recovered by suction sampler), and time (HHMM). The suction samples were processed immediately upon recovery on the ship. Excess seawater was poured off the sample container, and each sample was removed with sterile tools and placed on aluminum foil that was sterilized with ethanol. The samples were immediately photographed and placed in sterile Whirl-Pak® sample bags without allowing the samples to dry. Larger samples were stored as multiple aliquots of approximately 100 grams each in separate sample bags. The samples were placed in an −80 °C freezer within approximately 1 h of recovery on the ship.

The recovered samples are white to light yellow-brown, soft and friable, and show a porous structure. Upon recovery, all samples featured visible, mucilaginous textures (most likely indicative of biofilm growth) that coated all surfaces of the carbonate materials. When viewed shipboard, the biofilms have collapsed and do not resemble their *in situ* thickness, but seafloor video recordings indicate that these biofilms can extend >1 cm from the carbonate mineral substrate. Moreover, because the carbonate chimneys are highly porous, the biofilms are not restricted to the periphery of the chimney, and they appear to permeate the entire volume of the carbonate samples. Therefore, the word 'biofilm' in this article generally includes the carbonate structure infused with mucilaginous microbiological communities and is not restricted to a 'film' on the outer surface. Because they were collected off the surface of the chimneys where venting was observed, our samples are representative of very young deposits and are expected to predominantly record present-day processes at the interface between the hydrothermal fluids and seawater. After subsampling for our analyses, the samples were kept frozen at −20 °C and freeze-dried prior to lipid extraction.

Our samples thus differ from those investigated in the previous studies of Bradley *et al.* (2009a,b), which consisted of larger, intact carbonate chimney pieces sampled by the submersible *Alvin* in 2003 at the same vents and which are mainly representative of the bulk interior of the carbonate chimneys formed over time as the hydrothermal structures grow. In addition, we studied two samples collected in 2003 with *Alvin*. These samples were labeled according to *Alvin* dive number and time of collection (38XX-HHMM). The 2003 samples are large, intact segments of the carbonate chimneys, and much of the material was in contact with the vent fluids and can be considered similar to those studied in Bradley *et al.* (2009a,b).

Sample analysis

DNA fingerprinting of microbial communities

DNA was extracted from frozen carbonate chimney samples according to the previously published protocol of Brazelton *et al.* (2010a) except that three freeze–thaw cycles (−80 °C and 65 °C) were added before phenol extraction, and DNA extracts were purified for PCR amplification with QiaQuik columns (Qiagen) instead of dialysis. PCR amplification for TRFLP (terminal restriction fragment length polymorphism) was conducted with archaeal primers 21F ([6-FAM]TTCCGGTTGATCCYGCCGGA) and 958R (YCCGGCGTTGAMTCCAATT) and bacterial primers 27F ([6-FAM]AGAGTTTGATCCTGGCTCAG) and 1492R (GGTTACCTTGTTACGACTT) with the following cycling conditions: 94 °C for 5 min; 34 cycles of 94 °C for 30 s, 54 °C for 45 s, 72 °C for 2 min; and a final 72 °C extension for 10 min. Amplicons were purified with QIAquick columns and digested overnight with *Bst*UI, *Hae*III, *Msp*I, and *Rsa*I. Digested products were precipitated with ethanol and analyzed on an Applied Biosystems 3130 Genetic Analyzer at the East Carolina University Genomics Core Facility. Fragment sizes were taxonomically identified by comparison with predicted terminal restriction fragment sizes of sequences published in Brazelton *et al.* (2006). Positive identification required a match within ±1 bp confirmed by at least two restriction enzymes. Taxonomic classifications in Table 2 correspond to phylogenetic groups assigned by Brazelton *et al.* (2006).

Archaeal and bacterial 16S rRNA gene copy numbers were quantified by quantitative polymerase chain reaction (qPCR) of the DNA extracts described above. The following primers designed by the International Census of Marine Microbes were chosen for their known taxonomic specificities and their short amplicon lengths, thereby improving qPCR amplification efficiency: 967F and 1046R for bacteria; and 958F and 1048R for archaea. Primer sequences were published by Sogin *et al.* (2006) and are also available at http://vamps.mbl.edu/resources/primers.php.

Each qPCR was performed on a Bio-Rad CFX96 module and contained the following reagents: 5 μL water, 2 μL of each primer (5 μM), 10 μL of SsoFast Evagreen Supermix (Bio-Rad Laboratories, Hercules, CA, USA), and 1 μL of DNA template. Amplification consisted of 40 cycles of 2 s at 98 °C and 2 s at 57 °C after an initial denaturation step at 98 °C for 2 min. Starting quantities of 16S rRNA gene copies were calculated from the cycle number at which a threshold concentration (determined by default manufacturer software) was reached and calibrated with a standard curve generated by amplification with the same primers of genomic DNA from *Methanocaldococcus jannaschii* and *Escherichia coli* for archaea and bacteria,

Table 2 Identified microbial communities based on TRFLP analysis

Archaea	LC-Bh	LC-2b	LC-5	LC-7a	LC-7b	LC-Ha	LC-Cap
LCMS ANME1	Very low	Yes	Yes	Yes		Yes	Very low
Marine Group I	Yes	Yes	Yes	Yes	Yes	Yes	Yes
Bacteria							
Gram-positive Bacteria							
Desulfotomaculum				Yes			
Other Firmicutes	Yes			Yes		Yes	
Actinobacteria						Yes	
Nitrospira		Yes	Yes		Yes	Yes	Yes
CFB	Yes	Yes		Yes	Yes	Yes	
Planctomycetes		Yes				Yes	
Alphaproteobacteria		Yes	Yes	Yes	Yes	Yes	Yes
Betaproteobacteria				Yes			
Gammaproteobacteria							
Marinomonas	Yes	Yes	Yes	Yes	Yes	Yes	Yes
Methylobacter	Yes	Yes	Yes	Yes	Yes	Yes	Yes
Methylophaga	Yes	Yes		Yes		Yes	Yes
Thiomicrospira		Yes		Yes		Yes	
Animal symbiont			Yes	Yes	Yes	Yes	
Epsilonproteobacteria				Yes			

Yes = confirmed by 2 + restriction enzymes; very low = nearly below detection limit; blank = not detected.

respectively. The *M. jannaschii* and *E. coli* DNA standards were only amplified by their respective archaeal or bacterial primers, thus demonstrating the domain specificities of the primers. All samples were amplified as a dilution series to test for inhibition of amplification by contaminants. Data from the highest concentrations that showed minimal inhibition were selected for further analysis. Amplification efficiency was ~75% for all reactions reported here, and melt curve analysis indicated no significant contribution from non- specific products. Calculated starting 16S rRNA gene copy numbers were corrected for copy number in the standards (2 per *M. jannaschii* genome and 7 per *E. coli* genome) and normalized to the dry weight of the carbonate chimney material that was extracted, yielding 16S rRNA gene copies per gram of sample, and these results were used to calculate archaea/bacteria ratios for each sample. The relative standard deviation between three replicate qPCRs was less than 10% for each sample.

Bulk organic carbon isotope composition

For bulk organic carbon isotope measurements ($\delta^{13}C_{org}$), samples were ground into a powder, which was decarbonated in 2 N hydrochloric acid twice for 24 h, and homogenized after neutralization and drying (Kennedy *et al.*, 2005). Water-soluble organic matter is thus excluded from the bulk organic carbon values. $\delta^{13}C_{org}$ was measured using a Thermo Scientific Flash Elemental Analyzer 1112 connected in continuous flow to a Thermo Scientific Delta V Plus isotope ratio mass spectrometer. Average reproducibility of analyses, based on repeated measurements of laboratory standards calibrated to NBS 22 ($\delta^{13}C = -30.03‰$), is better than $\pm$ 0.2‰. The $\delta^{13}C$ values are reported in the conventional delta notation relative to VPDB.

Lipid extraction and separation

Samples (amounts given in Table 3) were ground into a powder and extracted by sonication using methanol (MeOH, three times), a mixture of dichloromethane (DCM) and MeOH (1:1, v/v, three times), and DCM (three times). The extracts recovered by centrifugation were combined and the solvents evaporated under reduced pressure. The organic extracts were fractionated over a silica gel column (SiO_2, pore size 60 Å, 40–63 μm particle size, activated at 120 °C for 4 h) successively using hexane/DCM (9:1, v/v), DCM/MeOH (7:3, v/v), and DCM/MeOH (1:1, v/v) as eluents allowing the recovery of three fractions of increasing polarity. The first apolar fraction is mainly composed of hydrocarbons. Alcohols, fatty acids, and diols are the main constituents of the second fraction (polar fraction 1). The last fraction (polar fraction 2) contains compounds of higher polarity and macromolecular material. In some cases (samples LC-Bh, LC-500, LC-5, LC-6, and LC-Cap), the initial separation of the organic extract into a less polar and more polar fraction (polar fraction 2) was performed on a SiO_2 column successively using DCM/MeOH (7:3, v/v) and DCM/MeOH (1:1, v/v) as eluents. The less polar fraction recovered after this purification step was further fractionated on a small SiO_2 column successively using hexane/DCM (9:1, v/v) and DCM/MeOH (7:3, v/v), yielding an apolar fraction (hydrocarbons) and a second fraction (polar fraction 1).

Chemical degradation and derivatization procedures

An aliquot of polar fraction 1 was hydrolyzed for 2 h at 120 °C with 2 mL of hydrochloric acid (HCl, 12 M) in MeOH (1:9, v/v). Subsequently, the fraction was

Table 3 Individual archaeal lipid abundances and $\delta^{13}C$ and δD values of the analyzed samples

	LC-Bh		LC-500		LC-2a			LC-2b		LC-6		LC-5		LC-7a		LC-7b			LC-Ha		LC-Hb		LC-Hc		LC-Cap	
Sample amount (g)	102.5		56.5		55.1			23.2		63.5		29.8		35.2		51.1			51.6		42		50		40.6	
Total lipids (μg/g)	1		7		37			67		168		423		178		18			46		14		8		6	
Individual lipids	Conc.	$\delta^{13}C$	Conc.	$\delta^{13}C$	Conc.	$\delta^{13}C$	δ D	Conc.	$\delta^{13}C$	Conc.	$\delta^{13}C$	Conc.	$\delta^{13}C$	Conc.	$\delta^{13}C$	Conc.	$\delta^{13}C$	δ D	Conc.	$\delta^{13}C$	Conc.	$\delta^{13}C$	Conc.	$\delta^{13}C$	Conc.	$\delta^{13}C$
PMI	0.002	n. det.	bdl		0.19	7.3	−260	0.79	6.8	0.07	n.det.	0.005	n.det.	0.05	4.9	0.14	7.5	−269	bdl		bdl		bdl		0.01	n.det.
PMI:1	bdl				0.04	5.9	−211	0.07	n.det.					0.01	n.det.	0.01	2.9	n.det.	bdl		bdl		bdl			
PMI:1	bdl				0.05	7.5		0.11	5.4					0.01	n.det.	0.02	7.1	n.det.	bdl		bdl		bdl			
PIM:3 + PMI:1	bdl				0.02	7.8	n.det.	0.04	7.0					0.01	n.det.	0.004	9.3	n.det.	0.005	n.det.	bdl		bdl		t.a.	
PMI:2	bdl				0.11	6.4	−244	0.19						0.04		0.02		n.det.	bdl		bdl		bdl			
PMI:2	bdl		ta		0.04	6.6	n.det.	0.05	8.0					0.01	−7.3	0.01	11.7	n.det.	bdl		bdl		bdl			
PMI1 + PMI:2	bdl				0.11	7.7	n.det.	0.25	8.7		0.3*			0.03		0.04		n.det.	0.01	−3.2	0.001	−3.3	bdl			
PMI3 + PMI:2	bdl				bdl			bdl			3.0*			0.06		bdl			bdl		bdl		bdl			
PMI:3	bdl				1.07	6.1	−227	1.74	6.1	1.23	−1.8*	0.05	2.5*	0.29	4.4	0.28	5.5	−273	0.19	−5.8	0.04	−6.9	bdl			
PMI:3 + PMI:4	bdl				bdl			bdl			3.3*			0.02	n.det.	bdl			bdl		bdl		bdl			
PMI:3	bdl				0.03	1.4	n.det.	0.05	12.7					0.03	n.det.	0.004	n.det.	n.det.	0.003	n.det.	bdl		bdl			
PMI:3 + PMI:2	bdl				0.11	13.7	n.det.	0.28						0.03	n.det.	0.04	12.1	n.det.	0.01	n.det.	bdl		bdl			
PMI:4	bdl				0.23	4.6	−171	0.43	4.2					0.14	0.3	0.09	5.3	n.det.	0.06	−12.3	0.01	−8.2	bdl			
PMI:4	bdl				0.01	−0.8	n.det.	0. 02	3.6					0.02	n.det.	0.01	n.det.	n.det.	bdl		bdl		bdl			
PMI:4	bdl				0.12	24.6	−152	0.21	22.7					0.9	14.7	0.03	20.2	n.det.	bdl		bdl		bdl			
PMI:5	bdl				0.17	3.7	−133	0.37	−1.3					0.25	−2.2	0.07	6.1	−191	0.14	−6.2	0.01	n.det.	bdl			
Squalane (Sq)	0.01	−9.1	bdl		0.05	−4.0	n.det.	0.19	−3.8	0.01	n.det.	bdl		0.04	n.det.	0.06	−7.0	−283	0.01	n.det.	bdl		0.01	n.det.	0.01	n.det.
Sq:1	bdl		bdl		0.02	−3.8	n.det.	0.05	n.det.			bdl		0.01	n.det.	0.002	n.det.	n.det.	bdl		bdl		bdl			
Sq:1 + Sq:2	bdl		bdl		0.004	n.det.	n.det.	0.03	n.det.			bdl		0.02	n.det.	0.01	n.det.	n.det.	bdl		bdl		bdl			
Sq:2	bdl		bdl		0.01	n.det.	n.det.	0.04	n.det.			bdl		0.03	n.det.	0.004	n.det.	n.det.	0.02	n.det.	bdl		0.003	n.det.		
Sq:3	bdl		bdl		0.004	n.det.	n.det.	0.02	n.det.			bdl		0.01	n.det.	bdl			bdl		bdl		bdl			
Sq:2	bdl		bdl		bdl			0.02	n.det.			bdl		0.02	n.det.	0.02	−4.1	n.det.	bdl		bdl		bdl			
Sq:4	bdl		bdl		0.02	8.2	n.det.	0.09	11.6			bdl		0.09	n.det.	0.01		n.det.	0.03	n.det.	0.002	n.det.	bdl			
Sq:3	bdl		bdl		bdl	−11.4	n.det.	0.02	n.det.			bdl		0.03	n.det.	0.002	n.det.	n.det.	bdl		bdl		bdl		t.a.	
Sq:3	bdl		bdl		bdl			0.03	n.det.	0.57	n.det.	bdl		0.04	n.det.	0.01	−3.0	n.det.	bdl		bdl		bdl			
Sq:4	bdl		bdl		0.02	−5.7	n.det.	0.08	1.3			bdl		0.03	n.det.	0.01		n.det.	bdl		bdl		bdl			
Sq:5	bdl		bdl		0.01	1.7	n.det.	0.05	2.6			bdl		0.12	−11.6	0.01	n.det.	n.det.	0.02	n.det.	bdl		bdl			
Sq:4	bdl		bdl		0.03	−5.4	n.det.	0.11				bdl		1.28		0.02	−10.1	n.det.	0.02	n.det.	bdl		bdl		t.a.	
Sq:5	bdl		bdl		0.02	−6.1	n.det.	0.05	−4.7			bdl		0.05	n.det.	0.01	n.det.	n.det.	bdl		bdl		bdl			
Sq:5	bdl		bdl		0.03	−3.8	n.det.	0.1	1.6			bdl		0.06	n.det.	0.02	0.6	n.det.	0.01	n.det.	bdl		bdl			
Sq:6	bdl		bdl		0.53	−3.1	−220	1.93	−9.0			bdl		5.51	−11.0	0.41	−3.9	−228	0.86	−13.2	0.08	−13.9	2.88	−12.4		
Archaeol	bdl		0.03	n.det..	0.21	n.det.	n.det.	0.26	n.det.	2.93	1.7	2.18	n.det.	1.67	n.det.	0.19	n.det.	n.det.	0.08	n.det.	0.01	n.det.	bdl		0.02	n.det.
Hydroxyar. (+diOH)	bdl		0.17	2.0	1.12	4.7	n.det.	2.76	−0.5	14.9	3.3	5.74	1.4	9.74	−0.6	1.62	n.det.	n.det.	0.82	−3.3	0.09	n.det.	bdl		bdl	
Diploptene	bdl		0.003	n.det.	0.79	−17.9	n.det.	0.55	−18.1	0.28	n.det.	0.93	−16.4	0.12	−19.7	0.01	−18.5	n.det.	0.60	−17.3	0.04	−21.2	0.08	n.det..	0.67	−13.8
Diplopterol	0.002	n.det.	0.01	n.det.	0.72	−17.0	n.det.	0.37	n.det.					0.53	n.det.	0.04	n.det.	n.det.	0.47	−16.0	0.05	n.det.	0.09	−16.9	0.09	n.det.
∑ZPMIs	0.002		ta		2.3	7.3		4.6	5.8	1.3		0.055		1.9	7.5	0.768	6.5		0.418	−6.9	0.061	−7.1	bdl		0.01	
∑ISqs	0.01	−9.1	bdl		0.748	−3.0		2.81	−6.5	0.58		bdl		7.34	−11.1	0.598	−4.2		0.97	−13.2	0.082	−13.9	2.893	−12.4	0.01	

Bdl, below detection limit; n.det., not determined; t.a., trace amount; concentration (conc.) in μg/g; $\delta^{13}C$ in ‰ (VPDB); δD in ‰ (VSMOW). PMI, pentamethylicosane; PMIx, pentamethylicosene with x double bonds; Sqx, squalenoid with x double bonds. *Value determined on-by the transformed unsaturated PMIs.

evaporated to dryness under a gentle stream of nitrogen (N_2). For samples LC-Bh, LC-500, LC-5, LC-6, and LC-Cap, acid hydrolysis was performed prior to separation of apolar compounds. Acetylated derivatives were prepared with acetic anhydride and pyridine, at room temperature overnight. For approximately 10 mg of sample, 0.5 mL of acetic anhydride and 0.5 mL of pyridine were used. Trimethylsilyl (TMS) derivatives were obtained using BSTFA (N,O-bis(trimethylsilyl)trifluoroacetamide / TMCS (trimethylchlorosilane) (99:1, Supelco) in pyridine, at 60 °C for 30 min. For approximately 10 mg of sample, 100 µl of silylating reagent was used. For sample LC-7b, acetates were analyzed before acid hydrolysis.

For samples LC-2b and LC-7b, acid hydrolysis of the previously separated apolar fraction was carried out to study its effect on polyunsaturated alkenes. Acid hydrolysis (MeOH/HCl) resulted in the degradation of the polyunsaturated isoprenoids present in the apolar fraction (i.e., PMIs and squalenoids) and yielded multiple isomerization and cyclization products, as evidenced by hydrogenation (H_2/PtO_2) and oxidative (RuO_4) treatment (Fig. 2).

Hydrogenation was performed on an aliquot of apolar fractions to reduce double bonds from unsaturated compounds. The aliquot was dissolved in ethyl acetate, and an equivalent volume of acetic acid was added. After addition of a catalytic amount of platinum (IV) oxide (PtO_2, Acros Organics), the mixture was immediately placed under a N_2 atmosphere and then under a H_2 atmosphere. The reaction was performed by refluxing the mixture for 3 h. Solvents were evaporated to dryness under reduced pressure. When compounds showing degrees of unsaturation (i.e., double bonds and/or cycles) were still detected after hydrogenation, RuO_4 degradation (after Adam *et al.*, 2006) was performed to confirm the presence of cyclic structures.

Analytical methods for individual lipids

GC-MS (gas chromatography–mass spectrometry) analysis was carried out on a Hewlett Packard 6890 gas chromatograph equipped with an on-column injector and a DB5 ms fused silica capillary column (30 m × 0.32 mm; 0.25 µm film thickness) using helium as carrier gas (1.7 mL/min) coupled to a Hewlett Packard 5973 mass selective detector

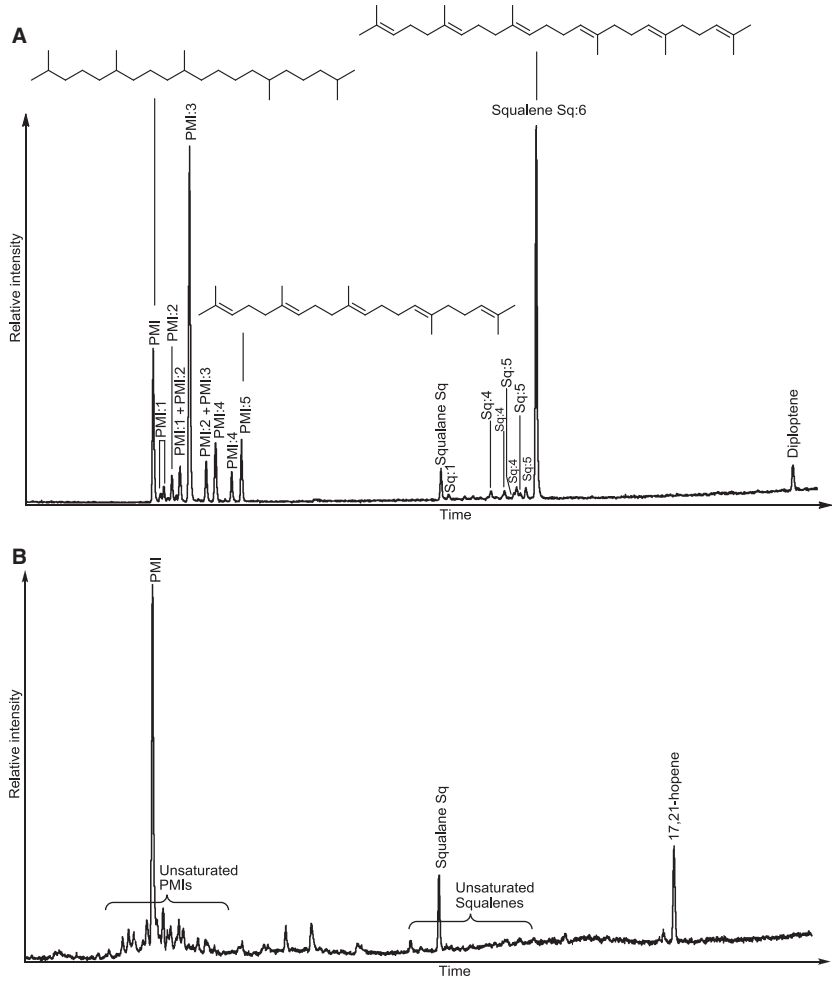

Fig. 2 Reconstructed ion chromatograms (RICs) of the apolar fraction of LC-2b (a) before and (b) after treatment with MeOH/HCl (9:1, v/v).

operating in electron impact mode (70 eV). The GC oven was programmed from 70 °C to 120 °C at 10 °C/min and then to 320 °C at 4 °C/min with an isothermal of 20 min at 320 °C. Abundances of compounds were determined on the reconstructed ion chromatogram. Quantification of individual lipids was based on the comparison of peak areas relative to the standards hexacosane (C_{26} *n*-alkane), triacontane (C_{30} *n*-alkane), 4-cholesten-3-one, and methyl octacosanoate (*n*-C_{28} fatty acid methyl ester).

Carbon and hydrogen isotopes ($\delta^{13}C$ and δD) were measured by gas chromatography/isotope ratio monitoring mass spectrometry (GC-irmMS). We used a Thermo Scientific system with a Trace GC Ultra, a GC IsoLink interface, a Conflo IV, and a Delta V Plus isotope ratio mass spectrometer. The GC equipped with a DB5 fused silica capillary column (30 m × 0.25 mm; 0.25 μm film thickness) was programmed from 70 °C to 120 °C at 10 °C/min and then to 300 °C at 3 °C/min with an isothermal of 30 min at 300 °C. Each sample was measured at least twice. $\delta^{13}C$ values are expressed in ‰ relative to VPDB. They have been corrected for carbon added during derivatization (acetate and TMS derivatives) and have an error of less than ±1‰. The error determination is based on analytical accuracy and precision of repeated measurements of laboratory standards calibrated to reference mixtures of *n*-alkanes provided by Arndt Schimmelmann (mixtures A2 and B2, Indiana University). δD values are expressed in ‰ relative to VSMOW and have an error of less than ±12‰, based on repeated measurements of standards calibrated to the previously mentioned reference mixtures A2 and B2.

Glycerol dibiphytanyl glycerol tetraethers (GDGTs) were analyzed by liquid chromatography/mass spectrometry (LC–MS) on a system consisting of a Finnigan Surveyor LC Pump Plus (Thermo Scientific) and a LCQ ion trap mass spectrometer equipped with an atmospheric pressure chemical ionization (APCI) source (Thermo Scientific). The analytical procedure was adapted from Hopmans *et al.* (2000) and Schouten *et al.* (2007). A Prevail Cyano column (2.1 × 150 mm, 3 μm; Alltech, Deerfield, Illinois, USA), maintained at 30 °C, was eluted using a linear gradient from hexane/isopropanol (IPA) (98.8:1.2, v/v) to 2% (v) of IPA over 39 min with a flow rate of 0.25 mL/min. Subsequently, a flow rate of 0.3 mL/min was used for 10 min. Then the linear gradient was set to 6.9% (v) of IPA at 0.25 mL/min for 5 min and at 0.3 mL/min for 5 min. Finally, the column was eluted with hexane/IPA (99:1, v/v) at 0.25 mL/min for 10 min. Detection was achieved using the positive ionization mode of the APCI. The APCI parameters were as follows: vaporizer temperature 300 °C, sheath gas (N_2) flow 40 (arb. units), auxiliary gas (N_2) flow 5 (arb. units), capillary temperature 200 °C, capillary voltage 23 V, source current 5 μA, and source voltage 6 kV. In some cases, single-ion monitoring (SIM) was used instead of full mass scanning to increase the signal-to-noise ratio. SIM was set to cover the mass range from m/z 1290 to 1304. MS/MS spectra were generated according to the procedure described in Knappy *et al.* (2009). The data-dependent ion scan feature was used, in which the base peak, namely the protonated molecular ion $[M + H]^+$ for GDGTs, was selected for collision-induced dissociation (CID). The collision energy was set to 30% and the isolation width to 3 m/z. For GDGT analysis, an aliquot of the polar fractions was dissolved in hexane/IPA (99:1, v/v) by sonication (10 min). After settling of the particles, supernatant was recovered and filtered through a 4-mm PTFE (0.45 μm) filter prior to LC-MS analysis.

RESULTS

DNA analysis

The microbial diversity of samples LC-Bh, LC-2b, LC-5, LC-7a, LC-7b, LC-Ha, and LC-Cap was assessed by terminal restriction fragment length polymorphism (TRFLP) analysis. Taxonomic identifications of TRFLP peaks are shown in Table 2. A TRFLP peak corresponding to *LCMS* archaea was dominant in samples LC-5, LC-7a, LC-Ha, and LC-2b, which is consistent with previous studies (Schrenk *et al.*, 2004; Brazelton *et al.*, 2006, 2010a). In LC-Cap and LC-Bh, however, the *LCMS* peak was much smaller than the Marine Group I *Crenarchaeota* peak, and *LCMS* peak was absent in LC-7b, which was a grab sample recovered by the submersible *Alvin* in 2003. Archaeal DNA from this sample was very poorly amplified by PCR and therefore had a very high detection limit, so it is possible that *LCMS* is present in LC-7b at low levels. More than sufficient DNA was recovered from this sample, so the poor amplification is due to the lack of archaeal DNA and/or to inhibition. DNA yields (per gram of extracted material) of LC-Cap and LC-Bh were 2–7 times lower than that for the other samples, which may reflect lower biomass. Unfortunately, no samples in this study were preserved for cell counts. No genetic diversity or taxonomic data from the chimneys where LC-Cap, LC-Bh, and LC-7b were collected have been previously published.

No evidence for ANME-1 was detected in any of the samples we investigated. This is consistent with previous TRFLP and 16S rDNA sequencing studies, which showed no ANME-1 in other samples from the same chimneys (Brazelton *et al.*, 2006). Sequences expected to represent bacterial methylotrophs (*Methylobacter* and *Methylophaga*) were identified with TRFLP peaks in all samples. This is consistent with the previous TRFLP study (Brazelton *et al.*, 2006), which detected bacterial methylotrophs in all samples, suggesting that they inhabit the periphery of chimney biofilms where methane and oxygen are available. Only three samples (LC-2b, LC-7a, LC-Ha) showed evidence for the sulfur-oxidizing clade *Thiomicrospira*, in

contrast with the previous study, which found *Thiomicrospira* in all LCHF carbonate chimneys and fluids. Overall, however, the taxonomic identifications from this study are in agreement with previously published microbiology data from LCHF carbonate chimneys (Brazelton *et al.*, 2006, 2010a). Nevertheless, it should be noted that all samples contained major bacterial TRFLP peaks (5–10 per sample, <40% of total peaks) that could not be identified with a sequence from the study by Brazelton *et al.* (2006); therefore, the taxonomic identifications in Table 2 do not represent an exhaustive census of microbial diversity, as is the case with any TRFLP study.

The abundance of archaeal and bacterial 16S rRNA genes was assessed with quantitative polymerase chain reaction (qPCR) measurements. The relative contribution of archaea to the total microbial population varied widely, from 1–81% (Fig. 3). Samples with low levels of archaeal 16S rRNA gene abundance (LC-Cap, LC-Bh, LC-7b) are also those in which a T-RFLP peak associated with the *LCMS* is very low or absent (Fig. 3).

Bulk organic carbon isotope composition

The carbon isotope composition ($\delta^{13}C_{org}$) of the total organic carbon ranges from −15.2‰ to −1.8‰, averaging −11.4‰ (Table 1). Large variations in $\delta^{13}C_{org}$ are found even for samples within the same carbonate–brucite chimneys. These variations were also observed by Kelley *et al.* (2005), Bradley *et al.* (2009a), and Lang *et al.* (2012) and reflect natural heterogeneities within a given carbonate tower. This is confirmed by the significant difference between the $\delta^{13}C$ values measured on two aliquots of the 64 g sample LC-6 (Table 1).

Lipid biomarkers

The total concentration of detected lipids per gram of samples varies widely from 1 μg/g to 423 μg/g (Table 3).

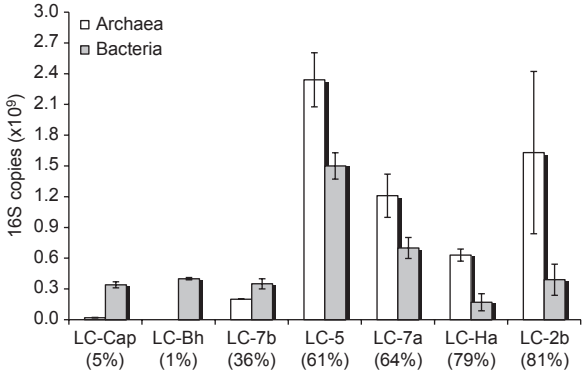

Fig. 3 Abundances of 16S copies as determined by qPCR. Error bars represent standard deviation of the measurement. The relative contribution of archaea (%) to the total population is reported below each sample name.

Archaeal biomarkers comprise C_{25} isoprenoids related to pentamethylicosane (PMI) and C_{30} isoprenoids related to squalane (Sq), glycerol diphytanyl diethers (archaeol and hydroxyarchaeols), and glycerol dibiphytanyl glycerol tetraethers (GDGTs). Bacterial biomarkers mainly include fatty acids, alcohols, hopanoids (diploptene, diplopterol), and a variety of non-isoprenoidal diethers from C_{33} to C_{38} (total number of carbon atoms), although the origin of the latter compounds remains to be confirmed (Bradley *et al.*, 2009b). Eukaryotic biomarkers such as cholesterol were also detected and reflect the contribution of pelagic microbial communities to the organic matter at the surface of the chimneys. As this study examines the role of archaea in the LCHF, in the following, we present the detailed description of the detected archaeal biomarkers with emphasis on their identification, distribution, and carbon and hydrogen isotope compositions ($\delta^{13}C$ and δD). Some non-archaeal biomarkers are succinctly described for the needs of the discussion.

In samples LC-Bh, LC-500, LC-5, LC-6, and LC-Cap, less than 20% of the original amount of polyunsaturated isoprenoids could be detected as well-defined peaks following acidic hydrolysis (see Materials and Methods).

Pentamethylicosane-related isoprenoids

Except in sample LC-Hc, all samples showed the presence of the saturated PMI and of isomeric mixtures of unsaturated PMIs with one to five double bonds. Structural identification of saturated PMI was based on the comparison of its mass spectrum with that of a synthetic standard (Risatti *et al.*, 1984). The presence of the double bonds in the unsaturated PMIs was confirmed by hydrogenation of apolar fractions, which yielded exclusively the saturated PMI. The mass spectrum of one particular tetra-unsaturated PMI (referred to as PMI:4*) showed a significant fragment at m/z 123, indicative of a PMI bearing a central saturated bond, previously described by Schouten *et al.* (1997) and Sinninghe Damsté *et al.* (1997).

The concentrations of all the identified PMIs are reported in Table 3, and representative chromatograms of PMI distributions are shown in Fig. 4. The concentration of PMIs varies from below detection limit (bdl) (sample LC-Hc) to 4.6 $\mu g/g_{sample}$ and represents up to 7% of the detected lipids. The $\delta^{13}C$ values of PMIs ($\delta^{13}C_{PMIs}$) (Table 3) range from −12.3‰ to +24.6‰, with large variations between samples, but also within each sample. PMI:4* shows the highest $\delta^{13}C$ of all the biomarkers detected in the Lost City samples (Table 3, see also Bradley *et al.*, 2009a), with values ranging from +14.7‰ to +24.6‰ and averaging +20.6‰.

The samples fall into three broad categories. In samples where PMI:4* can be detected, total PMI concentrations are high and their $\delta^{13}C$ values are more positive ($\delta^{13}C_{PMI}$ = −1.3‰ to +13.7‰; LC-2a, LC-2b, LC-7a,

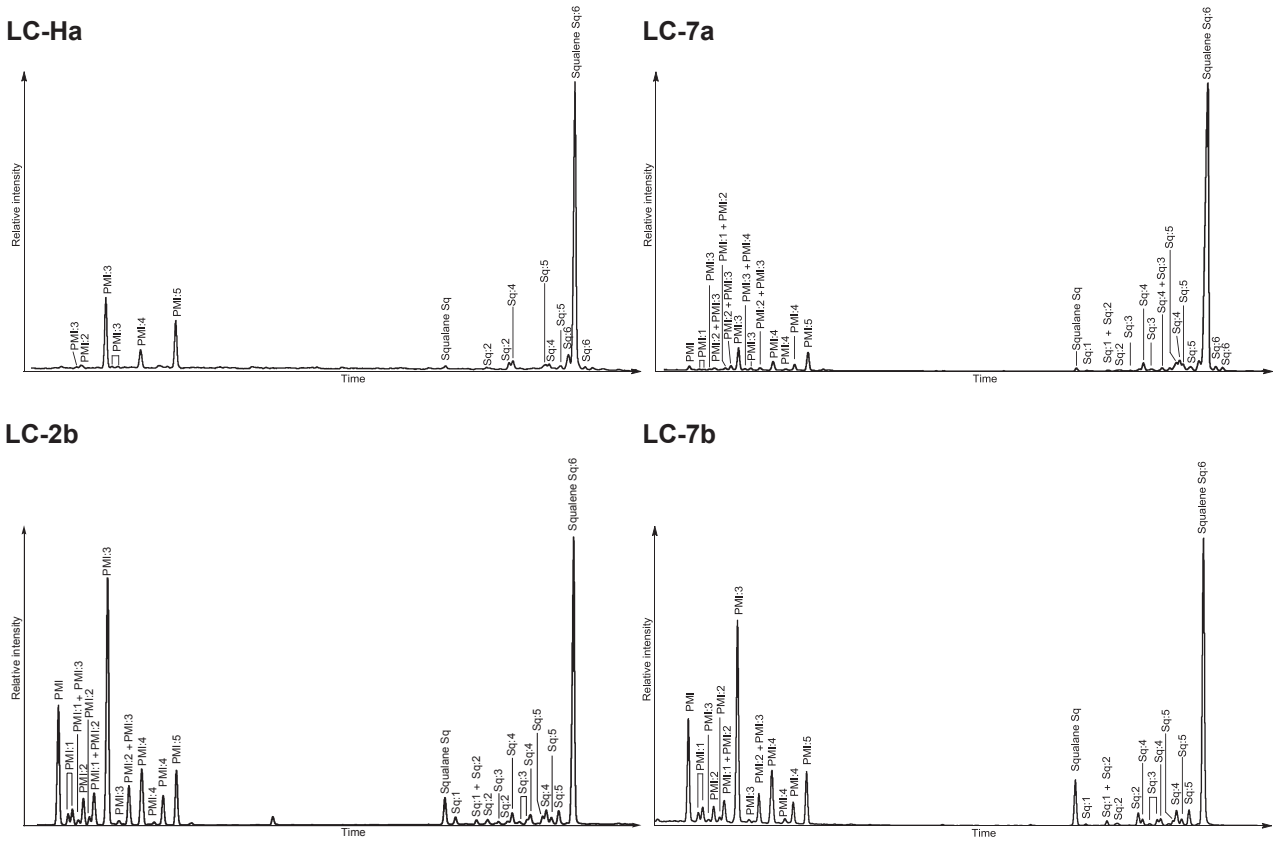

Fig. 4 Reconstructed ion chromatograms of the apolar fractions of four representative samples (LC-Ha, LC-2a, LC-7a, and LC-7b) showing distinct distributions of PMIs and squalenoids.

LC-7b). Two other samples (LC-5 and LC-6) are also tentatively assigned to this group based on the $\delta^{13}C$ values of the cyclized compounds resulting from MeOH/HCl treatment ($\delta^{13}C_{cyc}$ = −1.8 to +3.3 ‰). In the second group, PMI:4* is absent, and all other PMIs are in low concentrations and are more negative ($\delta^{13}C_{PMI}$ from −12.3‰ to −3.2‰, LC-Ha and LC-Hb). In the third group, PMIs are present only in trace amounts (LC-Bh, LC-500, LC-Cap) or were not detected (LC-Hc).

The δD_{PMIs} values for samples LC-2a and LC-7b range from −273‰ to −133‰ (Table 3). In both cases, the δD_{PMIs} values show a general decrease (values become more negative) with decreasing number of unsaturations.

Squalane-related isoprenoids (squalenoids, Sqs)

With the exception of samples LC-500 and LC-5, all samples contained squalane and unsaturated analogues with one to six unsaturations. The presence of double bonds rather than rings was confirmed by hydrogenation with H_2/PtO_2, which led exclusively to the formation of squalane. The concentration of all identified squalenoids is reported in Table 3, and representative chromatograms of their distributions are shown in Fig. 4. The concentration of squalenoids varies from bdl to 7.3 $\mu g/g_{sample}$ and represents up to 4% of the detected lipids, except in sample LC-Hc where it reaches 36%. In sample LC-Bh, squalane is the only detected squalenoid compound. Otherwise, squalene (Sq:6) is predominant, representing between 68 and 98% of the squalenoids, followed by squalane.

Similar to the PMI distributions, three groups of samples can be distinguished based on the squalenoid $\delta^{13}C$ values (Table 3). A first group has squalenoids with more positive $\delta^{13}C$ values ranging from −11.4‰ to +11.6‰ and averaging about −3‰ (samples LC-2a, LC-2b, and LC-7b). A second group has more negative $\delta^{13}C$ values around −13‰ (samples LC-Ha, LC-Hb, and LC-Hc) and shows the highest relative abundances of squalene. A third group has squalenoids present only in very low abundance (LC-Bh, LC-500, LC-5, and LC-Cap). Squalenoids from sample LC-7a have $\delta^{13}C$ values intermediate between the first two groups. In samples LC-2a and LC-2b, one Sq with four unsaturations has a particularly high $\delta^{13}C$ value at +8.2‰ and +11.6‰ compared with the $\delta^{13}C$ values of the Sqs detected in the other samples, respectively, and may be related to PMI:4*. Although the relative abundance of PMIs and squalenoids do not correlate (r^2 = 0.2), the concentration-weighted average $\delta^{13}C$ values of all PMIs ($\delta^{13}C_{PMIs}$) and of all squalenoids ($\delta^{13}C_{Sqs}$)

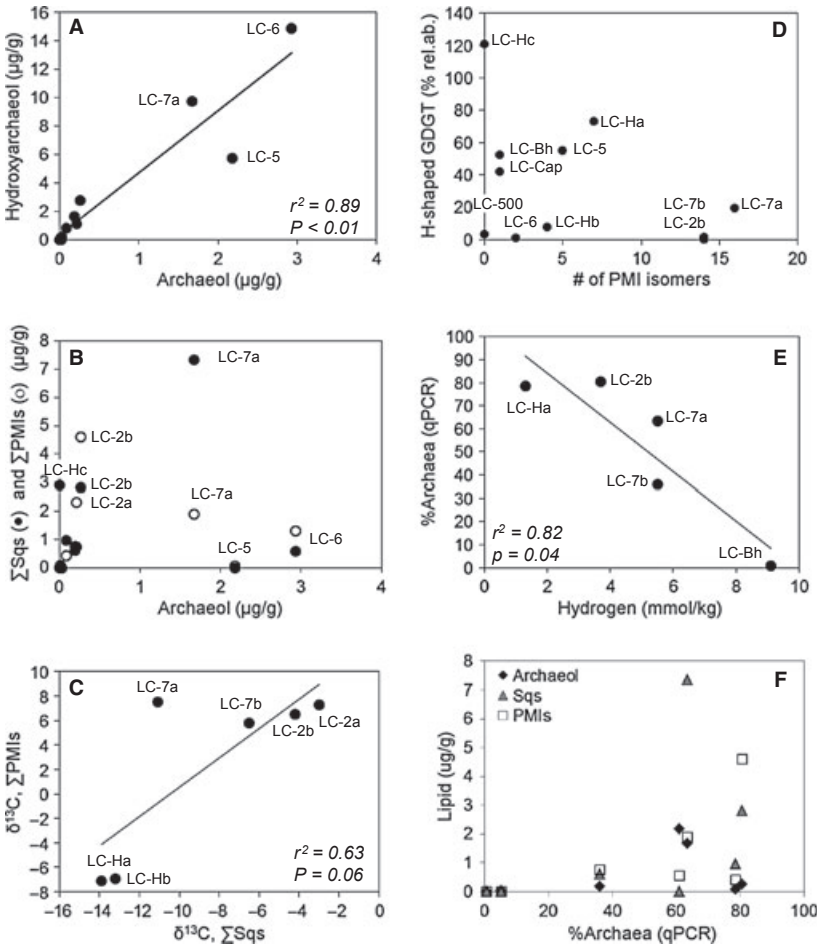

Fig. 5 Concentrations of (A) hydroxyarchaeol and (B) ∑PMIs and ∑Squalenoids vs. archaeol. (C) Average $\delta^{13}C$ composition (in ‰, VPDB) of ∑PMIs vs. ∑Squalenoids. Line represents least-squares fit of the data. (D) Relative abundance of H-shaped GDGT (normalized to the sum of GDGTs excluding the H-shaped GDGT, Fig. 6) vs. the number of detected PMI isomers. (E) Relative%Archaea in the microbial population as determined by qPCR vs. fluid endmember hydrogen concentrations from those chimneys. Hydrogen data from Proskurowski *et al.*, 2006. (F) Concentrations of archaeal lipids (archaeol, Sqs, PMIs) vs. the relative%Archaea in the microbial population as determined by qPCR.

show some positive correlation ($r^2 = 0.63$, $P = 0.06$), as shown in Fig. 5C.

Squalenoid δD values could be measured only in samples LC-2a and LC-7b and range from −283‰ to −220‰ (Table 3), with a general decrease to lower values with decreasing number of unsaturations.

Glycerol dibiphytanyl glycerol tetraethers

Glycerol dibiphytanyl glycerol tetraethers were identified based on their mass spectra, showing the protonated molecular ion $[M + H]^+$ as base peak and small fragments at $[M + H]^+$-18 and $[M + H]^+$-74, corresponding to the loss of water and part of the glycerol moieties, respectively, and on the comparison of their retention times with reference samples that have been characterized previously in the literature (e.g., Schouten *et al.*, 2002). These identifications were confirmed by MS/MS analysis and are in agreement with the data published by Knappy *et al.* (2009).

Glycerol dibiphytanyl glycerol tetraethers include caldarchaeol ($[M + H]^+$ = m/z 1302) and homologues showing up to 3 cyclopentane rings within biphytanyl chains. GDGTs with 4 or 5 cyclopentane rings were not detected. Crenarchaeol ($[M + H]^+$ = m/z 1292) was also detected with its regioisomer (Sinninghe Damsté *et al.*, 2002). The relative abundances of GDGT are very variable (Fig. 6); however, crenarchaeol is usually dominant, with caldarchaeol being sometimes as abundant as crenarchaeol (samples LC-2b, LC-5, LC-Ha, and LC-Hb).

In addition to these GDGTs, one compound was identified with a base peak at $[M+H]^+$ = m/z 1300 showing fragments with losses of 18 and 74 mass units characteristic of GDGTs and eluting right after the series of commonly described GDGTs (Knappy *et al.*, 2009). MS/MS analysis showed few fragments (m/z = 1281, 1263, 1245, 1243, 1225, 1207, 1189, and 1171), indicating the presence of a covalent carbon–carbon bond between the two biphytanyl chains in the molecule (Knappy *et al.*, 2009). The relative abundance of this H-shaped GDGT (Fig. 6) varies extensively from bdl (sample LC-7b) to being more abundant than all the other GDGTs in samples LC-Ha and LC-Hc.

Glycerol diphytanyl diethers

With the exception of samples LC-Bh and LC-Hc, all samples display the presence of bis-*O*-phytanyl-sn-2,3-glycerol diether (archaeol) identified as its trimethylsilyl (TMS) and

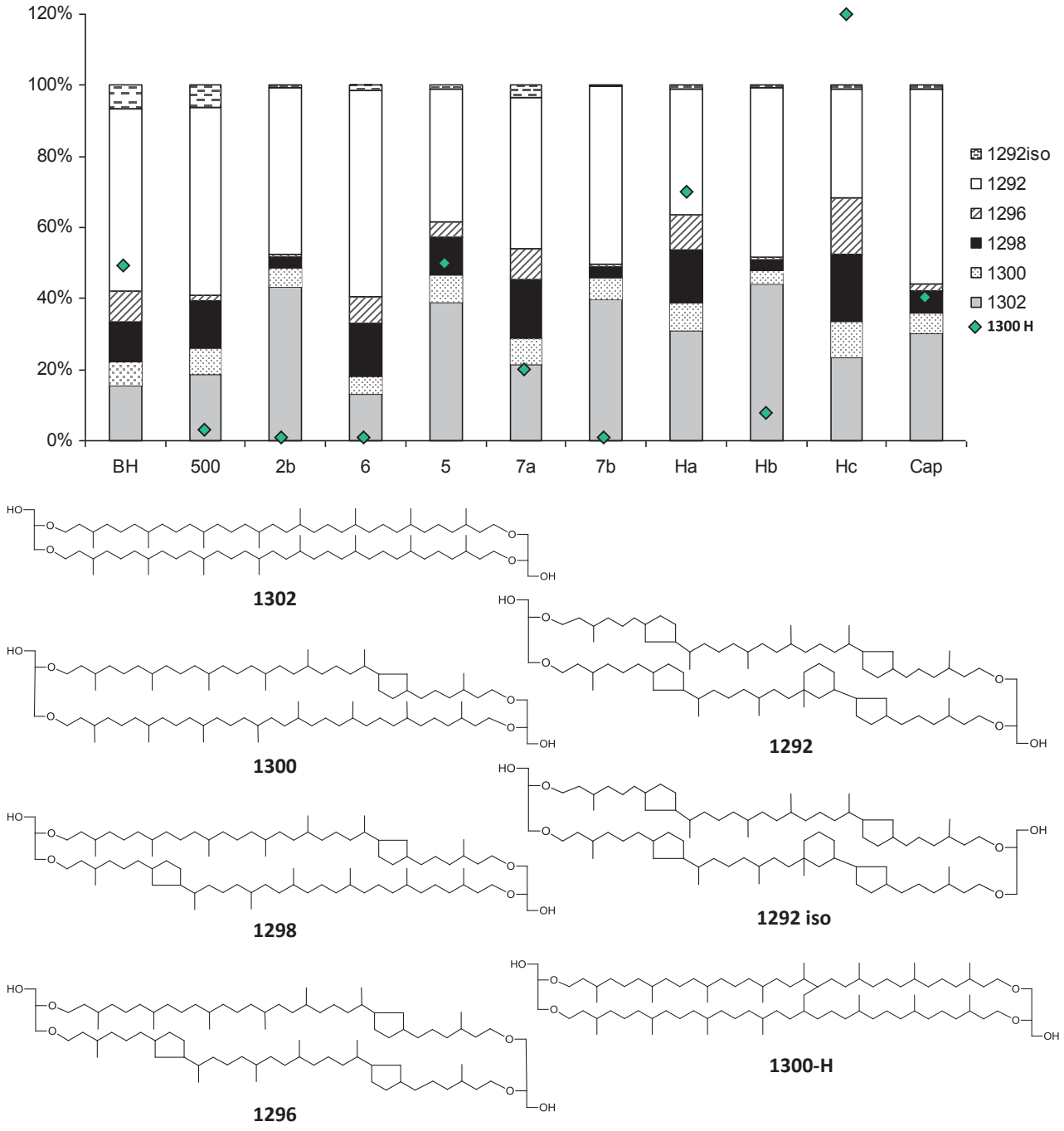

Fig. 6 Relative abundance of GDGTs with the exception of the H-shaped GDGT (1300 H). Diamonds represent the relative abundance of the H-shaped GDGT compared with the combined abundance of all other GDGTs. The *x*-axis bears the name of the samples as referred in the text as LC-sample name. Molecular structures of the GDGTs discussed in the text. H-shaped GDGT (1300 H) structure from Morii *et al.* (1998).

acetate derivatives, based on their mass spectra and comparison with the literature (Comita *et al.*, 1984; Teixidor & Grimalt, 1992). In sample LC-7b, which was not treated by MeOH/HCl, sn-2 and sn-3-hydroxyarchaeol were detected (as acetate derivatives) by comparing their mass spectra with those of reference standards (Sprott *et al.*, 1990; Hinrichs *et al.*, 2000).

Strong acid hydrolysis of hydroxyarchaeols results in their conversion into monophytanylglycerol and three major components, 3-methoxydiether, and cis/trans unsaturated isomers of phytanyl glycerol ether (Ekiel & Sprott, 1992). In the Lost City samples treated with MeOH/HCl, the original occurrence of hydroxyarchaeols prior to acid hydrolysis is evidenced by the detection of their converted

compounds showing loss of phytanylether-related fragments in their mass spectra (Liefkens *et al.*, 1979; Nichols *et al.*, 1993) and of phytadienes most probably originating from the 3-hydroxyphytanyl side chain of hydroxyarchaeols. The use of acid hydrolysis has revealed to be very destructive for the study of labile molecules and should be avoided, notably when compounds bearing (poly)unsaturations or tertiary hydroxyl groups are present (see Materials and Methods section). Unfortunately, given the small sample size, it was not possible to re-analyze the samples using a different procedure.

The degradation products of hydroxyarchaeols and possibly of dihydroxyarchaeol were present in all samples, except in samples LC-Bh, LC-Hc, and LC-Cap, in concentrations reaching up to 11% of the total detected lipids. When present, hydroxyarchaeols and dihydroxyarchaeol are 2 to 10 times more abundant than archaeol. The relative abundance of archaeol correlates well with the abundance of hydroxyarchaeol (Fig. 5A; $r^2 = 0.89$, $P < 0.01$), whereas the concentrations of squalenoids and PMIs do not correlate with that of archaeol (Fig. 5B). The $\delta^{13}C$ value of archaeol could only be measured in sample LC-6 (+1.7‰). In the other samples, the $\delta^{13}C$ values of hydroxyarchaeols were evaluated from those of their monophytanylglycerol derivatives and vary from −3.3‰ to +4.7‰, averaging +0.4‰, which is a narrower range compared with the $\delta^{13}C$ values of PMIs and squalenoids.

Non-archaeal biomarkers

Distributions of even carbon-numbered saturated fatty acids ranging from C_{14} to C_{26} were observed in all samples except sample LC-Bh. A high number of isomers were found including iso- and anteiso-fatty acids. In sample LC-Bh, the fatty acid distribution was limited to the C_{16} to C_{22} homologues. Mono- and di-unsaturated fatty acids were also present, but showed a simpler distribution, iso- and anteiso-fatty acids being notably absent. n-C_{16} and n-C_{18} fatty acids and their mono-unsaturated homologues were predominant in all samples. The total amounts of fatty acids ranged from 1 to 327 μg/g, averaging 50 μg/g, and showed a wide range of $\delta^{13}C$ values from −32.1‰ (sample LC-Hc) to −1.2‰ (sample LC-7a). For each sample, the spread in $\delta^{13}C$ values for the detected fatty acids was > 15‰.

Diploptene and diplopterol were the only detected hopanoids and were identified in all samples (Table 3) in concentrations ranging from 0.002 μg/g (sample LC-Bh) to 1.5 μg/g (sample LC-2a), averaging 0.5 μg/g. Within a sample, the $\delta^{13}C$ values of diploptene and diplopterol were similar, varying from −21.2‰ to −13.8‰ between the different samples. Various steroids including C_{27} to C_{30} sterols were also found and were studied in detail by Bradley *et al.* (2009a). In our samples, sterol $\delta^{13}C$ values ranged from −28.9‰ to −25.3‰.

DISCUSSION

The samples investigated in this study were collected by suction from the surface of actively venting carbonate chimneys, whereas other lipid studies of Lost City carbonate deposits to date (Bradley *et al.*, 2009a and b) were based on larger, bulk carbonate chimney pieces mainly representative of the less fragile, inner part of the carbonate chimneys. The DNA fingerprinting analyses (Table 2) confirm the presence of *LCMS* archaea and methylotrophic bacteria and the absence of ANME-1, consistent with previous reports of the microbial communities in the outer part of LCHF actively venting chimneys (Schrenk *et al.*, 2004; Brazelton *et al.*, 2006). In this environment, seawater infiltrates the porous structure of the carbonate towers leading to mixing with hydrothermal fluids. The chemical composition of the resulting fluid is strongly dependent on the degree of mixing and is therefore very difficult to assess. The degree of mixing varies according to the flow of the hydrothermal fluids, but also changes with the aging of chimneys, as older structures become less porous and less permeable than fresh ones. As a first approximation, we assume that the most exterior portions of the chimney experience the highest degree of seawater infiltration and mixing. In the following discussion, we integrate the genetic, molecular, and isotopic data to characterize the origin of the identified archaeal lipids in the carbonate deposits and the possible metabolism of archaea from which they derive.

Origin of the archaeal lipids

Origin of the isoprenoid hydrocarbons

Saturated and unsaturated C_{25} PMIs are usually considered as biomarkers for CH_4-metabolizing archaea (Holzer *et al.*, 1979; Brassell *et al.*, 1981; Blumenberg *et al.*, 2005). They have been identified in cultures (Schouten *et al.*, 1997) and in natural environments, such as methane seeps and carbonate crusts where archaea are believed to perform reverse methanogenesis as evidenced by low $\delta^{13}C$ values of the PMIs (e.g., Pancost *et al.*, 2001; Thiel *et al.*, 2001; Pape *et al.*, 2005; Bouloubassi *et al.*, 2006; Niemann & Elvert, 2008). The specific PMI:4* has also been detected at methane seeps (Elvert & Suess, 1999). Because the *LCMS* archaea are the only known CH_4-metabolizing archaea detected at Lost City, we infer that they are responsible for producing PMIs in the actively venting structures.

Squalane is a specific biomarker for archaea (Langworthy, 1985), and unsaturated squalenoids have been identified in methanogenic and halophilic archaea (Tornabene *et al.*, 1979; Stiehl *et al.*, 2005), suggesting that, at Lost City, squalenoids may also derive from *LCMS*. However, squalenoids are less common than PMIs in CH_4-rich environments where archaea are active (Wakeham *et al.*, 2007),

and based on their $\delta^{13}C$ signatures, they are not always attributed to archaeal precursors (Elvert *et al.*, 2000; Stadnitskaia *et al.*, 2005). In the Lost City chimneys, locations showing PMIs with the most positive $\delta^{13}C_{PMIs}$ values (LC-2a, LC-2b, LC-7a, LC-7b) are also associated with the presence of squalenoids displaying the most positive $\delta^{13}C_{Sqs}$ values (Fig. 5C). Both PMIs and squalenoids $\delta^{13}C$ values are more negative in two samples from the Marker H structure at the periphery of the hydrothermal field (LC-Ha and LC-Hb). Concentrations of both PMIs and squalenoids are very low or below detection limits in two locations (LC-Bh and LC-Cap), where the TRFLP and qPCR data indicate that *LCMS* is only present in very low abundance (Fig. 3, Table 2). The relationship between the taxonomic data and the concentrations of squalenoids together with the correlation between isotopic composition of the PMIs and of the squalenoids support that squalenoid compounds are produced by the *LCMS* (Figs. 5C,F).

Squalene is commonly found in prokaryotes and eukaryotes, and partly reduced squalene derivatives have been identified in bacteria (e.g., in *Streptomyces*; Olukoshi & Packter, 1994). At Lost City, the $\delta^{13}C$ values of steroids range from −28.9‰ to −25.3‰ and are significantly ^{13}C-depleted compared with the squalenoids (−13.9‰ to +11.6‰). Thus, we infer that squalenoids are not of eukaryotic origin. Diploptene and diplopterol are commonly found in sediments (e.g., Elvert *et al.*, 2001; Werne *et al.*, 2002; Sinninghe Damsté *et al.*, 2004; Blumenberg *et al.*, 2006) and have been attributed to a variety of aerobic and anaerobic bacteria (e.g., Rohmer *et al.*, 1984; Ourisson & Rohmer, 1992; Sinninghe Damsté *et al.*, 2007). Based on the results of the phylogenetic studies (Table 2; Schrenk *et al.*, 2004; Brazelton *et al.*, 2006), diploptene and diplopterol in our samples likely derive from the aerobic methanotrophs that have been identified in Lost City chimneys. Their $\delta^{13}C$ values (−21.2‰ to −13.8‰, Table 3) are consistent with such a possibility (Jahnke *et al.*, 1999), but this would imply that C-isotope fractionation is limited, as methane at Lost City has $\delta^{13}C$ values that range from −13.6‰ to −8.8‰ (Kelley *et al.*, 2005; Proskurowski *et al.*, 2008). Limited fractionation could result from factors such as high temperatures, locally low CH_4 availability, and the mode of carbon assimilation pathway used by the methanotrophic bacteria at Lost City (Jahnke *et al.*, 1999). For cultured bacterial methylotrophs, diploptene and diplopterol show $\delta^{13}C$ values up to 6‰ lower than that of squalene from which they derive, depending on growth conditions (Summons *et al.*, 1994). Thus, it cannot be excluded that bacterial methylotrophs could contribute, to some extent, to the unsaturated squalenoids in our samples. However, because the $\delta^{13}C$ values of the unsaturated squalenoids are in the same range or, in some cases, higher than those of squalane (Table 3), which is a typical archaeal lipid (Langworthy, 1985), the squalenoids at Lost City are most likely to be predominantly of archaeal origin, from the *LCMS* phylotype.

Origin of the tetraether lipids (GDGTs)

Glycerol dibiphytanyl glycerol tetraethers are diagnostic biomarkers for archaea (De Rosa *et al.*, 1986), but their structures vary widely between archaea and have been proved to be a useful tool to study species variability in a given environment. For certain archaea, the number of cyclopentane rings in the biphytanyl chains of GDGTs depends on growth conditions and environmental factors, such as pH and temperature (De Rosa *et al.*, 1986; Uda *et al.*, 2001; Schouten *et al.*, 2002; Macalady *et al.*, 2004). Other structural features, like the presence of one cyclohexane ring, have been attributed to specific archaea (e.g., Sinninghe Damsté *et al.*, 2002).

At Lost City, the distributions of GDGTs vary widely from site to site (Fig. 6). A high heterogeneity in GDGT distributions on a small scale has also been noted in terrestrial hot springs (Pearson *et al.*, 2008). At Lost City, the varying abundances of GDGTs might be related to a contribution of archaea of pelagic origin. However, the detection of crenarchaeol in a two-year-old chimney sample (LC-Bh: 91 °C, pH 10.7), where a pelagic contribution is rather unlikely, suggests that at least part of the GDGTs are produced within the LCHF.

The H-shaped GDGT has been identified in the hyperthermophilic archaea *Thermococcales* (Sugai *et al.*, 2004). Thermococcales were not detected in carbonate chimneys by this study or the previous study, but they have been identified in the LCHF fluids and are suspected to be present in the subseafloor (Brazelton *et al.*, 2006). The highest abundances (>40% relative to total GDGTs) of H-shaped GDGT are found in samples with relatively low numbers (i.e., less than 8) of PMI isomers (Fig. 5D), while, in contrast, those samples with the highest abundance of PMI isomers have a relatively low abundance of H-shaped GDGT (samples LC-2a, LC-7a, and LC-7b; Fig. 5D, Table 3). Thus, these lipids likely derive from distinct archaea. If H-shaped GDGT derives from subsurface Thermococcales, then these specific tetraethers probably reflect biomass contribution from organisms associated with hydrothermal fluids. The relative abundance of H-shaped GDGT compared with the overall abundance of the other GDGTs may therefore be indicative of the dominance of hydrothermal fluids and, in turn, of a low degree of seawater infiltration into the porous carbonate chimneys. This hypothesis is corroborated by the fact that sample LC-Hc shows the highest abundance of H-shaped GDGT. Indeed, this sample was collected in 2003 as an intact section of a carbonate chimney (not as a suction sample) and thus is expected to include more of the inner part of the chimney in contact with hydrothermal fluids than the other samples investigated in the present study.

Unfortunately, no TRFLP data are available from this sample.

Origin of the glycerol diphytanyl diethers

Archaeol is the most common and ubiquitous of the archaeal diethers. It has been identified in halophilic, thermophilic, and methanogenic archaea (De Rosa *et al.*, 1986). Hydroxyarchaeol is predominantly synthesized by archaea involved in the methane cycle (e.g., Sprott, 1992; Sprott *et al.*, 1993; Hinrichs *et al.*, 1999). Because of the analytical procedure that we used, and which resulted in the degradation of sn-2, sn-3, and dihydroxyarchaeol (see Materials and Methods section) in some of the investigated samples, the occurrence of hydroxyarchaeol is discussed here partly based on the previous lipid study of the Lost City carbonate chimneys by Bradley *et al.* (2009a) and on our samples that were not treated with hydrochloric acid (LC-2a, LC-2b, LC-7a, LC-7b, LC-Ha, LC-Hb, and LC-Hc). Sn-2 hydroxyarchaeol was found to be predominant, even relative to archaeol. The correlation between the relative abundances of archaeol and hydroxyarchaeol in the Lost City samples (Fig. 5A) suggests a common biological origin. In methane seep environments, a higher abundance of sn-2 hydroxyarchaeol is usually associated with the presence of ANME-2 or ANME-3 (Blumenberg *et al.*, 2004; Niemann & Elvert, 2008). However, as such archaea are absent at Lost City, *LCMS* archaea are the best candidates as the source organisms. Figure 5B shows, however, a poor correlation between the abundance of both PMIs and Sqs and that of archaeol. Under various environmental conditions, *LCMS* might be able to produce varying amounts of PMIs, Sqs, archaeol, and hydroxyarchaeol, likely as a response to environmental stress. This suggests that, for *LCMS* archaea, these families of lipids play a different physiological role, which remains to be understood.

Integrating microbiological and biomarker data

Regional variations in lipids and archaea

The fluids venting in the Lost City chimneys vary widely in their concentrations of H_2 (1–14 mmol/kg), SO_4^{2-} (1–3.7 mmol/kg), and HS^- (0.2–2.8 μmol/kg) (Kelley *et al.*, 2005; Proskurowski *et al.*, 2006; Lang *et al.*, 2012). Chimneys in the central portion of the field (Markers Bh, 500, 6) host fluids with higher temperatures (68–91 °C), higher H_2 concentrations, higher methane, higher SO_4^{2-} concentrations, and low HS^- concentrations. In these areas, mantle carbon has been shown to contribute to only ~10% of the biomass (Lang *et al.*, 2012). In contrast, chimneys on the periphery of the field (Markers 2, H, 7) host fluids with lower temperatures (47–62 °C), lower H_2 concentrations, lower methane, lower SO_4^{2-} concentrations, higher HS^- concentrations, and 50% chimney biomass synthesized from mantle carbon. The distributions of H_2, SO_4^{2-}, and HS^- have been attributed to varying degrees of microbial sulfate reduction, which is apparently limited in the higher-temperature fluids, but strongly impacts fluid chemistry in the lower-temperature fluids (Proskurowski *et al.*, 2006; Lang *et al.*, 2012). The fraction of the microbial community corresponding to archaea also varies widely within the Lost City chimneys, from 1–81% (Fig. 3). Interestingly, the relative abundance of archaea covaries with concentrations of hydrogen within the fluids, the lower abundances of H_2 (and therefore of SO_4^{2-}) in the fluids being positively correlated with the highest proportions of archaeal population (Fig. 5E; $r^2 = 0.82$, $P = 0.04$).

With the exception of the marker H sample, the locations that have high relative abundances of archaea are those which show the highest concentrations of PMIs and Sqs (LC-2a, LC-2b, LC-7a) (Fig. 5F). At sites LC-Bh and LC-Cap, the concentrations of both PMIs and squalenoids derived from LCMS are extremely low or below detection limits, likely as a result of unfavorable environmental conditions. At the beehive structure, fluid flow rates and fluid temperatures (91 °C) may indeed be too high to be conducive to the growth of this particular species. At the other end of the spectrum, the carbonate cap (LC-Cap) is exposed to minimal and/or diffuse hydrothermal fluid flow. The supply of electron donors potentially utilized by the LCMS (H_2, CH_4) may be insufficient for *LCMS* growth in this location.

Extraordinary high carbon isotope values of Lost City Methanosarcinales lipids

Fractionation of carbon during lipid biosynthesis depends on the isotope composition of the carbon source, substrate availability, and the biosynthetic pathways involved in carbon assimilation (Londry *et al.*, 2008 and references therein). High $\delta^{13}C$ values at Lost City have been interpreted to result from a restricted availability of the carbon source (Bradley *et al.*, 2009a). The LCHF is an extreme environment for microbial life, not only because of high pH and temperature conditions, but also because the vent fluids are limited in oxidized carbon (e.g., $\sum CO_2$) even if electron donors (H_2, CH_4) are abundant. The essential nutrients for life may also be limiting; while there is evidence that nitrogen is readily available, possibly due to nitrogen fixation (Brazelton *et al.*, 2011; Lang *et al.*, 2013), there are also indications that phosphorous may be limiting (Bradley *et al.*, 2009b). The *LCMS* archaea grow in biofilms attached to the hydrothermal deposits (Schrenk *et al.*, 2004; Brazelton *et al.*, 2006). This biofilm mode of growth may be a way to adapt to warm temperature, high pH, extreme redox conditions, and low levels of nutrients (Stewart, 2003).

Methanosarcinales are a diverse group of CH_4-metabolizing archaea (Schrenk *et al.*, 2004), with a high potential of

adaptation to diverse environments. Some *Methanosarcinales* are also known to be part of a consortium involved in anaerobic oxidation of methane (AOM; Knittel & Boetius, 2009 and references therein). Methanogenesis is accompanied by a C-isotope fractionation of 15–20‰, although cultivation experiments indicate that fractionation may be reduced under conditions of high H_2 concentration, high pressure, and high temperature (Londry *et al.*, 2008; Takai *et al.*, 2008). In the Lost City chimneys, the paucity of CO_2 ($\sum CO_2 = 0.1$ to 26 μmol/kg, with $\delta^{13}C_{\sum CO2}$ estimated to be approximately −9‰; Proskurowski *et al.*, 2008) likely leads to carbon limitation, which would also result in suppression of C-isotope fractionation (Bradley *et al.*, 2009a). After methane, formate is the second most abundant carbon species (36 to 158 μmol/kg) and the most dominant species contributing to dissolved organic carbon (DOC) in the fluids ($\delta^{13}C_{DOC} = -12.6$‰; Lang *et al.*, 2010; whereby DOC does not include CH_4) and can become a carbon source for methanogenesis, especially if seawater infiltration into the hydrothermal deposits is limited. Methane concentrations in the Lost City hydrothermal fluids range from 1 to 2 mmol/kg, and thus, methane is not expected to be limited within the carbonate towers. In addition, archaeal biomarkers related to methanotrophy are usually characterized by a substantial ^{13}C-depletion of −12‰ to −74‰ compared with the methane source (e.g., Elvert & Suess, 1999; Hinrichs *et al.*, 1999; Orphan *et al.*, 2002). At Lost City, given the methane abundance and $\delta^{13}C_{CH4}$ values of −13‰ to −9‰ (Kelley *et al.*, 2005; Proskurowski *et al.*, 2008), one may consider it unlikely for archaeal methanotrophy to lead to ^{13}C-enriched archaeal biomarkers.

If polyisoprenoid hydrocarbons and glycerol diphytanyl diethers can confidently be attributed to the *LCMS* archaea, neither equilibrium isotopic fractionation of any of the envisaged carbon sources nor the related metabolisms (methanogenesis/methanotrophy) can easily explain the $\delta^{13}C$ values observed for these lipids. High lipid $\delta^{13}C$ values of up to +24.6‰ on the outer chimney surfaces must, in part, be due to C-limitation and Rayleigh distillation and/or due to unusual isotopic fractionation during biosynthesis under these environmental conditions.

Controls on diversity of isoprenoid hydrocarbons

The C_{25} and C_{30} isoprenoid hydrocarbons at Lost City are characterized by an atypical variety of isomers with various degrees of unsaturation (Table 1, Fig. 2). These compounds, in particular PMIs, are frequently observed in CH_4-rich environments, and the number of double bonds has been postulated to be related to the methane flux, which can increase organic matter preservation by creating anoxic conditions (Elvert *et al.*, 2000). At Lost City, the distinct patterns of unsaturation between PMIs and squalenoids, for example, the presence of three isomers of squalene (Sqs:6) as opposed to a single isomer of PMI:5 (sample LC-7a, Fig. 2), suggests that the degree of unsaturation and the variety of isomers are linked to biosynthetic pathways and not to diagenetic alteration. The general trend of increasing δD values with increasing degree of unsaturation for both PMIs and squalenoids (Table 3) further supports a biosynthetic (vs. diagenetic) origin (Sessions *et al.*, 1999; Chikaraishi *et al.*, 2009). Indeed, archaeal isoprenoids are biosynthesized via the mevalonate pathway, a specific enzyme being responsible for the reduction in the isoprenoids (Nishimura & Eguchi, 2006), and likely favoring the enrichment in light hydrogen. On the contrary, reduction in hydrocarbon unsaturations during organic matter diagenesis is expected to be associated with increasing δD values (Schimmelmann *et al.*, 2006). At methane seeps, unsaturated PMI:4 and PMI:5 have been reported to be associated with ANME-3 methanotrophs (Niemann *et al.*, 2006), whereas a whole range of saturated and unsaturated PMIs with one to five unsaturations have been detected in *Methanosarcinales* ANME-1 and ANME-2 (Blumenberg *et al.*, 2004). However, ANME-2 may predominantly synthesize PMI:3 and PMI:4 (Nauhaus *et al.*, 2007). It is unclear whether these trends can be applied to all environments where ANMEs occur, especially considering their close phylogenetic relationships with each other. Generally, the distribution of the isomers of PMIs may be more related to the growth phase of the cell (Tornabene *et al.*, 1979) or to a response to different environmental factors (Lanyi *et al.*, 1974; Van de Vossenberg *et al.*, 1998) rather than to a taxonomic affiliation.

In addition to varying isomer distributions, the Lost City isoprenoids have highly heterogeneous $\delta^{13}C$ values. This is especially striking within individual samples, for example, sample LC-2a where the $\delta^{13}C_{PMI:4*}$ is 15‰ more positive than the other PMIs (Table 3). Similar heterogeneities in $\delta^{13}C_{PMIs}$ values have been observed at methane seeps and are attributed to heterogeneity in archaeal assemblages (Werne and Sinninghe Damsté, 2004; Stadnitskaia *et al.*, 2005; Bouloubassi *et al.*, 2006). In the Lost City actively venting carbonate towers, the only CH_4-metabolizing archaea are *LCMS*. This conclusion is drawn from the TRFLP data in this study (Table 2) and from TRFLP and sequencing data in previous studies (Brazelton *et al.*, 2006, 2010a,b). Although deep sequencing data are not yet available for the samples in this study, a prior study (Brazelton *et al.*, 2010a) assigned the *LCMS* phylotype to >90% of the 16 360 archaeal tag sequences from sample 3881-1408, which was collected from the same chimney structure as the LC-500 sample from this study. No other known methanogens were identified in any of the samples (corresponding to 167 031 archaeal tag sequences) in that study, indicating that multiple archaeal species cannot account for the diversity in isomers and $\delta^{13}C$ values.

Some of the variations in lipid isotope signatures may, in part, be due to unusual isotopic fractionations during biosynthesis under high H_2 concentrations leading to differences in ^{13}C values between archaeol and PMIs as large as 8–20‰ (Londry *et al.*, 2008). However, this difference in $\delta^{13}C$ values may also partly result from the presence of the glycerol group in archaeol. At Lost City, large variations in $\delta^{13}C$ values of PMIs and squalenoids unusual fractionation patterns for close biomarker families may have taken place to a certain extent. More likely, if the PMIs and Sqs complex distributions record the adaptation of the LCMS archaea to various environmental factors, their $\delta^{13}C$ values may also reflect a response to a change in the local environmental conditions. Biofilms are known to support diverse phenotypes even among genetically identical or highly similar organisms (Stoodley *et al.*, 2002; Boles *et al.*, 2004; Brazelton and Baross, 2009). Even though the Lost City biofilms are dominated by *LCMS*, they have surprising physiological complexity, including multiple cell morphologies (Brazelton *et al.*, 2011). Additionally, incubation experiments with these biofilms indicate that the *LCMS* may be capable of both methanogenesis and methanotrophy, suggesting that this single species of *Methanosarcinales* may have differentiated into multiple physiological roles (Brazelton *et al.*, 2011). It is unclear whether these phenotypes would be generated by genetically identical organisms or by differentiated, but still closely related, subpopulations such as those detected by

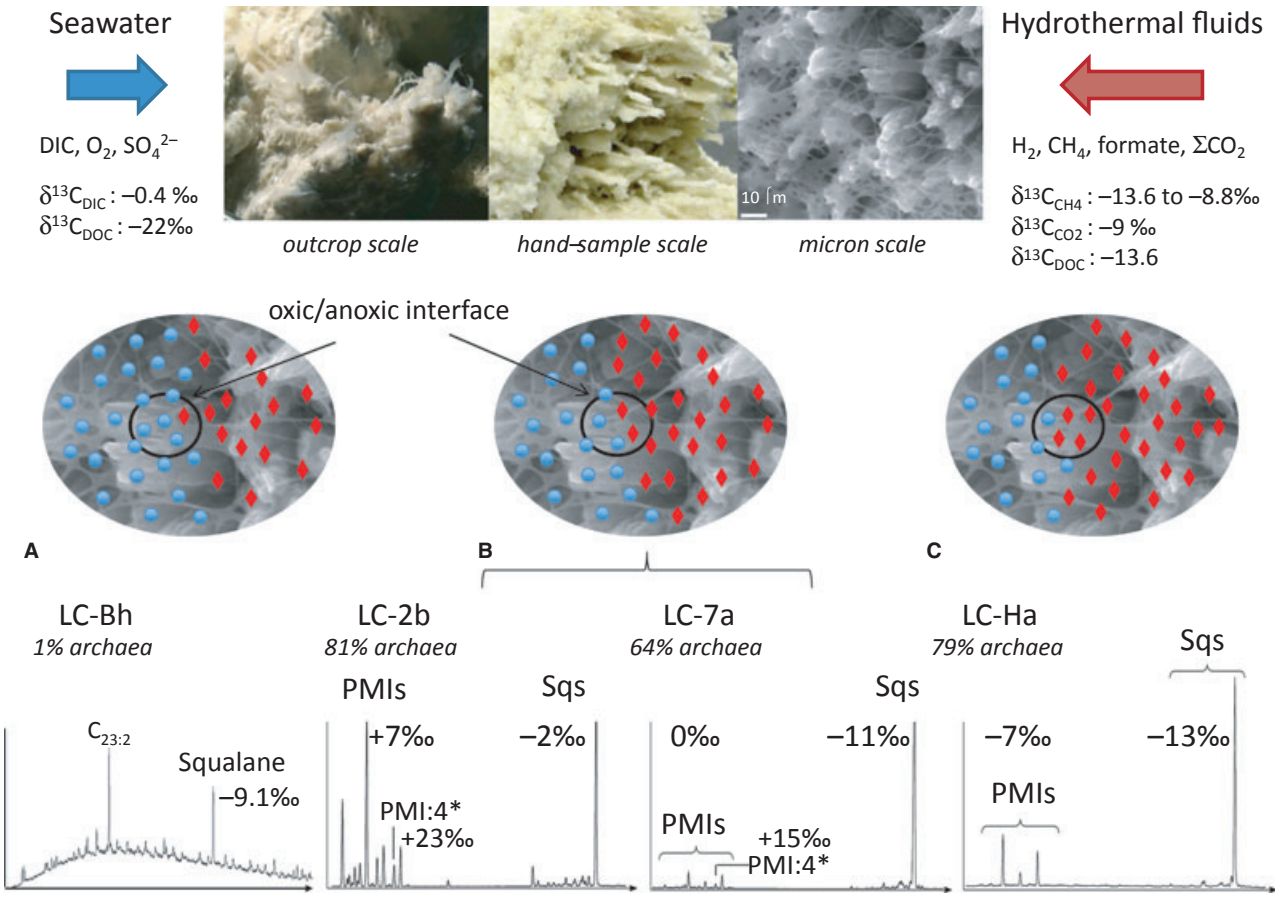

Fig. 7 Schematic diagram showing variations in environmental conditions and microbial activity at the oxic/anoxic interface where seawater and hydrothermal fluids mix in the porous carbonate–brucite structures (of the LCHF, see pictures in the upper part of the figure) and which lead to varying polyisoprenoid hydrocarbon distributions and archaeal abundances. The middle part of the figure shows a micrometer-scale model of this oxic/anoxic interface with diamonds representing the hydrothermal fluids and the circles representing seawater. Situation (A) corresponds to a young and highly porous chimney vigorously venting hydrothermal fluids associated with a low contribution of *LCMS* archaea likely feeding on the seawater carbon species compatible with the low incorporation of mantle carbon in the sedimentary organic matter found in this specific area (e.g., LC-Bh sample; Lang *et al.*, 2012). Situation (B) corresponds to an exterior part of an older chimney with a substantial contribution of seawater where a high diversity of *LCMS* phenotypes may thrive in response to the chemical gradients developing in these areas (e.g., LC-2b and LC-7a, see also Fig. 4). PMIs and Sqs show a high diversity in distribution and an extended range of $\delta^{13}C$ values possibly related to the biofilm mode of growth of the LCMS archaea (see Discussion). Situation (C) pictures a zone where hydrothermal fluid contribution is high such as close to the basement (Mkr H) preventing LCMS archaea to flourish and leading to a restricted distribution of PMIs and Sqs with lighter $\delta^{13}C$ values due to slightly less limiting carbon source availability.

DNA sequencing (Schrenk *et al.*, 2004; Brazelton *et al.*, 2010b). The structural and isotopic diversity in the archaeal lipids may reflect the multiple physiological and metabolic niches occupied by the Lost City *Methanosarcinales*.

The diversity in archaeal abundances, lipid structures and carbon isotope compositions, detected only in this series of samples that are believed to be representative mainly of the outermost part of the carbonate–brucite chimneys, may be related to the mixing interface of seawater and hydrothermal fluids where the *LCMS* archaea are able to adapt to strong chemical gradients in the hydrothermal chimneys. At this oxic/anoxic interface, carbon uptake will primarily be influenced by the availability and diffusion of methane or formate from the hydrothermal fluids and DIC from seawater within the biofilm (Fig. 7). At the high pH typical of the venting fluids, much of the seawater DIC is deposited as carbonate, and thus, the amount of carbon available for microbial activity will depend on the degree of mixing (Table 4). The biofilm mode of growth of the *LCMS* may help preserve anaerobic conditions in the exterior portions of the chimneys. *Methanosarcinales* strains are known to actively mitigate oxidative stress to preserve anaerobic activity (Brioukhanov *et al.*, 2000). In addition, aerobic bacteria, including methanotrophs, are abundant in domains where hydrothermal fluids mix with seawater (Schrenk *et al.*, 2004) and would contribute to maintaining locally low levels of oxygen.

Regardless of which carbon substrate is considered (CO_2, formate, CH_4), as ^{12}C is consumed faster than ^{13}C at the periphery of the biofilm, the isotopic composition of the biomass at the oxic/anoxic interface will be controlled by diffusion as well as by Rayleigh distillation within the biofilm, leading to the biosynthesis of lipids progressively enriched in ^{13}C. In addition, structural changes may occur by an adaptation to more stressful environmental conditions within the biofilm and would contribute to the variety of PMIs and squalenoids recorded in our samples. Figure 7 sketches a model showing how various degrees of mixing between seawater and hydrothermal fluids may influence the *LCMS* biofilm and the resulting archaeal lipid distribution and $\delta^{13}C$ values. As Sqs are relatively ^{13}C-depleted compared with PMIs, suggesting a shorter diffusion step, the archaea directly at the oxic/anoxic interface in the outer part of the biofilm might preferentially synthesize squalenoids. More stressful environmental conditions, characterized by carbon limitation, a longer diffusion step, and/or greater reaction progress, would result in the production of PMIs with a ^{13}C-enriched composition. The PMI:4* with $\delta^{13}C$ values of up to +24.6‰ may typify particularly substrate-starved archaea in the inner part of the biofilm. Further studies on the biofilm mode of growth are needed to assess this hypothesis. However, the unprecedented variations in the distributions and C-isotope values of structurally close compounds associated with a single species presented in this article are consistent with the drastic environmental condition gradients in the Lost City carbonate chimneys.

Lost City *Methanosarcinales* can perform both methanotrophy and methanogenesis, and it seems likely that this particular species has been developing several phenotypes at Lost City as a response to the chemical and temperature gradients, especially in the exterior parts of the chimneys. The high variability in the *LCMS* archaeal lipid record may reflect the presence of multiple *LCMS* phenotypes. PMIs and Sqs distribution and isotope values are likely to vary as a response to environmental changes (Fig. 7), which may play a key role in the capability of the LCMS archaea to thrive in Lost City hydrothermal chimneys.

CONCLUSIONS

Our studies reveal the presence of a variety of archaeal and bacterial biomarkers at the Lost City hydrothermal field. In the porous outer parts of the carbonate chimneys, variations in hydrothermal fluid flow allow for more or less extensive seawater infiltration, creating an interface where specific microbial biofilm communities can develop. Microbiological data together with the lipid distributions and their compound-specific carbon isotope compositions indicate that this habitat primarily supports CH_4-oxidizing bacteria and the CH_4-cycling archaeon *LCMS*.

Table 4 Estimated composition of the media resulting from mixing between hydrothermal fluids and seawater with increasing degree of seawater infiltration

	No seawater infiltration	10% seawater infiltration	50% seawater infiltration	90% seawater infiltration	Extinct
$\sum CO_2$ (μmol/kg)*	<0.1 to 26	~215	~1055	~1890	2100
$\sum CO_2 \delta^{13}C$ (‰)*†	−8.7	−8.2	−5.8	−1.8	−0.4
Formate (μmol/kg)‡	36 to 158	32 to 142	18 to 79	3.6 to 16	0
Acetate (μmol/kg)‡	1 to 35	0.9 to 31.5	0.5 to 17.5	0.1 to 3.5	0
DOC $\delta^{13}C$ (‰)‡	−12.6	−13.1	−15.6	−20.5	−22.5
CH_4 (μmol/kg)‡	1000–2000	900–1800	500–1000	100–200	0
CH_4 $\delta^{13}C$ (‰)‡	−13.6 to −9.3	−13.6 to −9.3	−13.6 to −9.3	−13.6 to −9.3	−13.6 to −9.3

*From Proskurowski *et al.* (2008). †Calculated as ideal mixing between seawater (21 mmol/kg, −0.4%) and hydrothermal (4 μmol/kg, −8.7%) fluids. ‡From Lang *et al.* (2010).

This study reveals the extraordinary heterogeneity in the C_{25} and C_{30} polyisoprenoid hydrocarbon (PMIs and squalenoids) distributions and in their $\delta^{13}C$ composition, showing values ranging from −11.4‰ to +24.6‰. PMIs and squalenoids at Lost City were found to derive from the *LCMS* archaea. Variations in $\delta^{13}C$ values in archaeal biomarkers most probably deriving from single species could result from unusual isotopic fractionation in this particularly stressful environment. However, the diversity in PMI and squalenoid distributions and $\delta^{13}C$ values is rather proposed to reflect the ability of the *LCMS* archaea to adapt to conditions where carbon is limited. The specific biofilm mode of growth of the archaeal *LCMS* likely contributes to the heterogeneity observed in the lipid distributions. The integration of microbiological studies and archaeal biomarker data also indicates that the extent of seawater mixing with the hydrothermal fluids may be recorded in the relative abundance of the unusual H-shaped GDGT, possibly produced in the subseafloor by *Thermoccocales*.

The *LCMS* archaea may be capable of CH_4 production and consumption as a mechanism to adapt to the different extreme biochemical niches encountered at Lost City. We argue that the structural diversity in the PMIs/squalenoids detected in our study probably reflects this versatility. A deeper knowledge of the physiological role of these specific lipid biomarkers may help to unravel the question as to why so many different PMIs and squalenoids are produced and in response to which factors.

ACKNOWLEDGMENTS

We thank Deborah S. Kelley, Giora Proskurowski, and the participants of the 2005 NOAA Ocean Explorer and the 2003 R/V Atlantis AT-7-41 cruises. We would particularly like to thank Marvin D. Lilley for constructive discussions and his contribution to earlier versions of the manuscript. Chantal Ulmer, Rienk Smittenberg, Maria Coray-Strasser, and Stewart Bishop provided valuable assistance with the analyses. We would also like to thank the reviewers for constructive comments that contributed to improving the manuscript. This work was supported by Swiss National Science Foundation Grants 200021-121840 and 20020-131922 to Früh-Green and Bernasconi. This work was also supported by a NASA Astrobiology Institute grant to Schrenk (Cooperative Agreement NNA04CC09A) through the Carnegie Institution for Science. Brazelton was supported by a NASA Astrobiology Institute postdoctoral fellowship.

REFERENCES

Adam P, Schaeffer P, Albrecht P (2006) C_{40} monoaromatic lycopane derivatives as indicators of the contribution of the alga *Botryococcus braunii* race L to the organic matter of Messel oil shale (Eocene, Germany). *Organic Geochemistry* **37**, 584–596.

Allen DE, Seyfried WE (2004) Serpentinization and heat generation: constraints from Lost City and Rainbow hydrothermal systems. *Geochimica et Cosmochimica Acta* **68**, 1347–1354.

Blumenberg M, Seifert R, Reitner J, Pape T, Michaelis W (2004) Membrane lipid patterns typify distinct anaerobic methanotrophic consortia. *Proceedings of the National Academy of Sciences USA* **101**, 11111–11116.

Blumenberg M, Seifert R, Nauhaus K, Pape T, Michaelis W (2005) In vitro study of lipid biosynthesis in an anaerobically methane-oxidizing microbial mat. *Applied and Environmental Microbiology* **71**, 4345–4351.

Blumenberg M, Kruger M, Nauhaus K, Talbot HM, Oppermann BI, Seifert R, Pape T, Michaelis W (2006) Biosynthesis of hopanoids by sulfate-reducing bacteria (genus *Desulfovibrio*). *Environmental Microbiology* **8**, 1220–1227.

Boles BR, Thoendel M, Singh PK (2004) Self-generated diversity produces "insurance effects" in biofilm communities. *Proceedings of the National Academy of Sciences USA* **101**, 16630–16635.

Bouloubassi I, Aloisi G, Pancost RD, Hopmans EC, Pierre C, Sinninghe Damsté JS (2006) Archaeal and bacterial lipids in authigenic carbonate crusts from eastern Mediterranean mud volcanoes. *Organic Geochemistry* **37**, 484–500.

Bradley AS, Summons RE (2010) Multiple origins of methane at the Lost City Hydrothermal Field. *Earth and Planetary Science Letters* **297**, 34–41.

Bradley AS, Hayes JM, Summons RE (2009a) Extraordinary ^{13}C enrichment of diether lipids at the Lost City Hydrothermal Field indicates a carbon-limited ecosystem. *Geochimica et Cosmochimica Acta* **73**, 102–118.

Bradley AS, Fredricks H, Hinrichs K-U, Summons R (2009b) Structural diversity of diether lipids in carbonate chimneys at the Lost City Hydrothermal Field. *Organic Geochemistry* **40**, 1169–1178.

Brassell SC, Wardroper AMK, Thomson ID, Maxwell JR, Eglinton G (1981) Specific acyclic isoprenoids as biological markers of methanogenic bacteria in marine sediments. *Nature* **290**, 693–696.

Brazelton WJ, Baross JA (2009) Abundant transposases encoded by the metagenome of a hydrothermal chimney biofilm. *The International Society for Microbial Ecology Journal* **3**, 1420–1424.

Brazelton WJ, Schrenk MO, Kelley DS, Baross JA (2006) Methane- and sulfur-metabolizing microbial communities dominate the Lost City Hydrothermal Field ecosystem. *Applied and Environmental Microbiology* **72**, 6257–6270.

Brazelton WJ, Ludwig KA, Sogin ML, Andreishcheva EN, Kelley DS, Shen C-C, Edwards RL, Baross JA (2010a) Archaea and bacteria with surprising microdiversity show shifts in dominance over 1,000-year time scale in hydrothermal chimneys. *Proceedings of the National Academy of Sciences USA* **107**, 1612–1617.

Brazelton WJ, Sogin ML, Baross JA (2010b) Multiple scales of diversification within natural populations of archaea in hydrothermal chimney biofilms. *Environmental Microbiology Reports* **2**, 236–242.

Brazelton WJ, Mehta MP, Kelley DS, Baross JA (2011) Physiological differentiation within a single-species biofilm fueled by serpentinization. *mBio* **2**, e00127-11.

Brioukhanov A, Netrusov A, Sordel M, Thauer RK, Shima S (2000) Protection of *Methanosarcina barkeri* against oxidative stress: identification and characterization of an iron superoxide dismutase. *Archives of Microbiology* **174**, 213–216.

Chikaraishi Y, Tanaka R, Tanaka A, Ohkouchi N (2009) Fractionation of hydrogen isotopes during phytol biosynthesis. *Organic Geochemistry* **40**, 569–573.

Comita PB, Gagosian RB, Pang H, Costello CE (1984) Structural elucidation of a unique macrocyclic membrane lipid from a new, extremely thermophilic, deep-sea hydrothermal vent archaebacterium, *Methanococcus jannaschii. Journal of Biological Chemistry* **259**, 15234–15241.

De Rosa M, Gambacorta A (1988) The lipids of archaebacteria. *Progress in Lipid Research* **27**, 153–175.

De Rosa M, Gambacorta A, Gliozzi A (1986) Structure, biosynthesis and physicochemical properties of archaebacterial lipids. *Microbiological Reviews* **50**, 70–80.

Ekiel I, Sprott GD (1992) Identification of degradation artifacts formed upon treatment of hydroxydiether lipids from methanogens with methanolic hydrochloric acid. *Canadian Journal of Microbiology* **38**, 764–768.

Elvert M, Suess E (1999) Anaerobic methane oxidation associated with marine gas hydrates: superlight C-isotopes from saturated and unsaturated C_{20} and C_{25} irregular isoprenoids. *Naturwissenschaften* **86**, 295–300.

Elvert M, Suess E, Greinert J, Whiticar M (2000) Archaea mediating anaerobic methane oxidation in deep-sea sediments at cold seeps of the eastern Aleutian subduction zone. *Organic Geochemistry* **31**, 1175–1187.

Elvert M, Greinert J, Suess E, Whiticar M (2001) Carbon isotopes of biomarkers derived from methane-oxidizing microbes at Hydrate Ridge, Cascadia convergent margin. In *Natural Gas Hydrates: Occurrence, Distribution, and Detection* (eds Paull C, Dillon W). Geophysical Monograph Series 124, American Geophysical Union, Washington, DC, pp. 115–129.

Früh-Green GL, Kelley DS, Bernasconi SM, Karson JA, Ludwig KA, Butterfield DA, Boschi C, Proskurowski G (2003) 30,000 years of hydrothermal activity at the Lost City Vent Field. *Science* **301**, 495–498.

Früh-Green GL, Connolly JAD, Plas AP, Kelley DS, Grobéty B (2004) Serpentinization of oceanic peridotites: Implications for geochemical cycles and biological activity. In *The Subseafloor Biosphere at Mid-Ocean Ridges. Geophysical Monograph Series* (eds Wilcock WSD, Baross JA, Kelly DS, DeLong EF, Cary C). American Geophysical Union, Washington, DC, pp. 119–136.

Gliozzi A, Paoli G, De Rosa M, Gambacorta A (1983) Effect of isoprenoid cyclization on the transition temperature of lipids in thermophilic archaebacteria. *Biochimica et Biophysica Acta* **735**, 234–242.

Hinrichs K-U, Hayes JM, Sylva SP, Brewer PG, DeLong EF (1999) Methane-consuming archaebacteria in marine sediments. *Nature* **398**, 802–805.

Hinrichs K-U, Summons RE, Orphan V, Sylva SP, Hayes J (2000) Molecular and isotopic analysis of anaerobic methane-oxidizing communities in marine sediments. *Organic Geochemistry* **31**, 1685–1701.

Holm NG, Charlou J-L (2001) Initial indications of abiotic formation of hydrocarbons in the Rainbow ultramafic hydrothermal system, Mid-Atlantic Ridge. *Earth And Planetary Science Letters* **191**, 1–8.

Holzer G, Oro J, Tornabene TG (1979) Gas chromatographic-mass spectrometric analysis of neutral lipids from methanogenic and thermoacidophilic bacteria. *Journal of Chromatography* **186**, 795–809.

Hopmans EC, Schouten S, Pancost RD, van der Meer MTJ, Sinninghe Damsté JS (2000) Analysis of intact tetraether lipids in archaeal cell material and sediments by high performance liquid chromatography/atmospheric pressure chemical ionization mass spectrometry. *Rapid Communications in Mass Spectrometry* **14**, 585–589.

Jahnke LL, Summons RE, Hope JM, Des Marais DJ (1999) Carbon isotopic fractionation in lipids from methanotrophic bacteria II: the effects of physiology and environmental parameters on the biosynthesis and isotopic signatures of biomarkers. *Geochimica et Cosmochimica Acta* **63**, 79–93.

Janecky DR, Seyfried WEJ (1986) Hydrothermal serpentinization of peridotite within the oceanic crust: experimental investigations of mineralogy and major element chemistry. *Geochimica et Cosmochimica Acta* **50**, 1357–1378.

Kelley DS, Karson JA, Blackman DK, Früh-Green GL, Butterfield DA, Lilley MD, Olson EJ, Schrenk MO, Roe KK, Lebon GT, Rivizzigno P, and the ATSP (2001) An off-axis hydrothermal vent field near the Mid-Atlantic Ridge at 30°N. *Nature* **412**, 145–149.

Kelley DS, Karson JA, Früh-Green GL, Yoerger DR, Shank TM, Butterfield DA, Hayes JM, Schrenk MO, Olson EJ, Proskurowski G, Jakuba M, Bradley A, Larson B, Ludwig KA, Glickson D, Buckman K, Bradley AS, Brazelton WJ, Roe K, Elend MJ, Delacour A, Bernasconi SM, Lilley MD, Baross JA, Summons RE, Sylva S (2005) A serpentinite-hosted ecosystem: the Lost City Hydrothermal Field. *Science* **307**, 1428–1434.

Kennedy P, Kennedy H, Papadimitriou S (2005) The effect of acidification on the determination of organic carbon, total nitrogen and their stable isotopic composition in algae and marine sediment. *Rapid Communications in Mass Spectrometry* **19**, 1063–1068.

Knappy CS, Chong JPJ, Keely BJ (2009) Rapid discrimination of archaeal tetraether lipid cores by liquid chromatography-tandem mass spectrometry. *Journal of the American Society for Mass Spectrometry* **20**, 51–59.

Knittel K, Boetius A (2009) Anaerobic oxidation of methane: progress with an unknown process. *Annual Review of Microbiology* **63**, 311–334.

Lang SQ, Butterfield DA, Schulte M, Kelley DS, Lilley MD (2010) Elevated concentrations of formate, acetate and dissolved organic carbon found at the Lost City hydrothermal field. *Geochimica et Cosmochimica Acta* **74**, 941–952.

Lang SQ, Früh-Green GL, Bernasconi SM, Lilley MD, Proskurowski G, Méhay S, Butterfield DA (2012) Microbial utilization of abiogenic carbon and hydrogen in a serpentinite-hosted system. *Geochimica et Cosmochimica Acta* **92**, 82–99.

Lang SQ, Früh-Green GL, Bernasconi SM, Butterfield DA (2013) Sources of organic nitrogen at the serpentinite-hosted Lost City hydrothermal field. *Geobiology* **11**, 154–169.

Langworthy TA (1985) Lipids of archaebacteria. In *The Bacteria-A Treatise on Structure and Function, Volume 8: Archaebacteria* (eds Woese CR, Wolfe RS). Academic Press, New York, NY, USA, pp. 459–497.

Lanyi JK, Plachy WZ, Kates M (1974) Lipid interactions in membranes of extremely halophilic bacteria. II. Modification of the bilayer structure by squalene. *Biochemistry* **13**, 4914–4920.

Liefkens W, Boon JJ, de Leeuw JW (1979) On the occurrence of alkyl- and alk-1-enyl-diacylglycerides in the lugworm *Arenicola marina*. *Netherlands Journal of Sea Research* **13**, 479–486.

Londry KL, Dawson KG, Grover HD, Summons RE, Bradley AS (2008) Stable isotope fractionation between substrates and products of *Methanosarcina barkeri*. *Organic Geochemistry* **39**, 608–621.

Ludwig KA, Kelley DS, Butterfield DA, Nelson BK, Früh-Green GL (2006) Formation and evolution of carbonate chimneys at the Lost City Hydrothermal Field. *Geochimica et Cosmochimica Acta* **70**, 3625–3645.

Ludwig KA, Shen C-C, Kelley DS, Cheng H, Edwards RL (2011) U-Th systematic and ^{230}Th ages of carbonate chimneys at the Lost City Hydrothermal Field. *Geochimica et Cosmochimica Acta* **75**, 1869–1888.

Macalady JL, Vestling MM, Baumler D, Boekelheide N, Kaspar CW, Banfield JF (2004) Tetraether-linked membrane monolayers in Ferroplasma spp a key to survival in acid. *Extremophiles* **8**, 411–419.

McCollom TM (2007) Geochemical constraints on sources of metabolic energy for chemolithoautotrophy in ultramafic-hosted deep-sea hydrothermal systems. *Astrobiology* **7**, 933–950.

McCollom TM, Bach W (2009) Thermodynamic constraints on hydrogen generation during serpentinization of ultramafic rocks. *Geochimica et Cosmochimica Acta* **73**, 856–879.

Morii H, Eguchi T, Nishihara M, Kakinuma K, Konig H, Koga Y (1998) A novel ether core lipid with H-shaped C_{80}-isoprenoid hydrocarbon chain from the hyperthermophilic methanogen *Methanothermus fervidus*. *Biochimica et Biophysica Acta* **1390**, 339–345.

Nauhaus K, Albrecht M, Elvert M, Boetius A, Widdel F (2007) In vitro cell growth of marine archaeal-bacterial consortia during anaerobic oxidation of methane with sulfate. *Environmental Microbiology* **9**, 187–196.

Nichols PD, Shaw PM, Mancuso CA, Franzmann PD (1993) Analysis of archaeal phospholipid-derived di- and tetraether lipids by high temperature capillary gas chromatography. *Journal of Microbiological Methods* **18**, 1–9.

Niemann H, Elvert M (2008) Diagnostic lipid biomarker and stable carbon isotope signatures of microbial communities mediating the anaerobic oxidation of methane with sulphate. *Organic Geochemistry* **39**, 1668–1677.

Niemann H, Lösekann T, de Beer D, Elvert M, Nadalig T, Knittel K, Amann R, Sauter EJ, Schlüter M, Klages M, Foucher J-P, Boetius A (2006) Novel microbial communities of the Haakon Mosby mud volcano and their role as methane sink. *Nature* **443**, 854–858.

Nishimura Y, Eguchi T (2006) Digeranylgeranylglycerophospholipid reductase. *The Journal of Biochemistry* **139**, 1073–1081.

Olukoshi ER, Packter NM (1994) Importance of stored triacylglycerols in *Streptomyces*: possible carbon source for antibiotics. *Microbiology* **140**, 931–943.

Orphan VJ, House CH, Hinrichs K-U, McKeegan KD, DeLong EF (2002) Multiple archaeal groups mediate methane oxidation in anoxic cold seep sediments. *Proceedings of the National Academy of Sciences USA* **99**, 7663–7668.

Ourisson G, Rohmer M (1992) Hopanoids. 2. Biohopanoids: a novel class of bacterial lipids. *Accounts of Chemical Research* **25**, 403–408.

Pancost RD, Hopmans EC, Sinninghe Damsté JS, and the Medinaut Shipboard Scientific Party (2001) Archaeal lipids in Mediterranean cold seeps: molecular proxies for anaerobic methane oxidation. *Geochimica et Cosmochimica Acta* **65**, 1611–1627.

Pape T, Blumenberg M, Seifert R, Egorov VN, Gulin SB, Michaelis W (2005) Lipid geochemistry of methane-seep-related Black Sea carbonates. *Palaeogeography Palaeoclimatology Palaeoecology* **227**, 31–47.

Pearson A, Pi Y, Zhao W, Li W, Li Y, Inskeep W, Perevalova A, Romanek C, Li S, Zhang CL (2008) Factors controlling the distribution of archaeal tetraethers in terrestrial hot springs. *Applied and Environmental Microbiology* **74**, 3523–3532.

Proskurowski G, Lilley MD, Kelley DS, Olson EJ (2006) Low temperature volatile production at the Lost City Hydrothermal Field, evidence from a hydrogen stable isotope geothermometer. *Chemical Geology* **229**, 331–343.

Proskurowski G, Lilley MD, Seewald JS, Früh-Green GL, Olson E, Lupton JE, Sylva SP, Kelley DS (2008) Abiogenic hydrocarbon production at Lost City Hydrothermal Field. *Science* **319**, 604–607.

Risatti JB, Rowland SJ, Yon DA, Maxwell JR (1984) Stereochemical studies of acyclic isoprenoids – XII. Lipids of methanogenic bacteria and possible contributions to sediments. *Organic Geochemistry* **6**, 93–104.

Rohmer M, Bouvier-Nave P, Ourisson G (1984) Distribution of hopanoid triterpenes in prokaryotes. *Journal of General Microbiology* **130**, 1137–1150.

Schimmelmann A, Sessions AL, Mastalerz M (2006) Hydrogen isotopic (D/H) composition of organic matter during diagenesis and thermal maturation. *Annual Review of Earth and Planetary Sciences* **34**, 501–533.

Schouten S, van der Maarel MJEC, Huber R, Sinninghe Damsté JS (1997) 2,6,10,15,19-Pentamethylicosenes in *Methanolobus bombayensis*, a marine methanogenic archaeon, and in *Methanosarcina mazei*. *Organic Geochemistry* **26**, 409–414.

Schouten S, Hopmans EC, Schefuß E, Sinninghe Damsté JS (2002) Distributional variations in marine crenarchaeotal membrane lipids: a new tool for reconstructing ancient sea water temperatures? *Earth and Planetary Science Letters* **204**, 265–274.

Schouten S, Huguet C, Hopmans EC, Kienhuis MVM, Sinninghe Damsté JS (2007) Improved analytical methodology and constraints on analysis of the TEX_{86} paleothermometer by high performance liquid chromatography/atmospheric pressure chemical ionization-mass spectrometry. *Analytical Chemistry* **79**, 2940–2944.

Schrenk MO, Kelley DS, Bolton SA, Baross JA (2004) Low Archaeal diversity linked to subseafloor geochemical processes at the Lost City Hydrothermal Field, Mid-Atlantic Ridge. *Environmental Microbiology* **6**, 1086–1095.

Sessions AL, Burgoyne TW, Schimmelmann A, Hayes JM (1999) Fractionation of hydrogen isotopes in lipid biosynthesis. *Organic Geochemistry* **30**, 1193–1200.

Sinninghe Damsté JS, Schouten S, Herbert van Vliet N, Huber R, Geenevasen JAJ (1997) A polyunsaturated irregular acyclic C_{25} isoprenoid in a methanogenic archaeon. *Tetrahedron Letters* **38**, 6881–6884.

Sinninghe Damsté JS, Hopmans EC, Schouten S, van Duin ACT, Geenevasen JAJ (2002) Crenarchaeol: the characteristic glycerol dibiphytanyl glycerol tetraether membrane lipid of cosmopolitan pelagic Crenarchaeota. *Journal of Lipid Research* **43**, 1641–1651.

Sinninghe Damsté JS, Rijpstra WIC, Strous M, Jetten MSM, David ORP, Geenevasen JAJ, van Maarseveen JH (2004) A mixed ladderane/n-alkyl glycerol diether membrane lipid in an anaerobic ammonium-oxidizing bacterium. *Chemical Communications* **22**, 2590–2591.

Sinninghe Damsté JS, Rijpstra WIC, Schouten S, Fuerst JA, Jetten MSM, Strous M (2007) The occurrence of hopanoids in planctomycetes: implications for the sedimentary biomarker record. *Organic Geochemistry* **35**, 561–566.

Sogin ML, Morrison HG, Huber JA, Mark Welch D, Huse SM, Neal PR, Arrieta LM, Herndl GJ (2006) Microbial diversity in the deep sea and the underexplored "rare biosphere". *Proceedings National Academy of Science* **103**, 12115–12120.

Sprott GD (1992) Structures of archaebacterial membrane lipids. *Journal of Bioenergetics and Biomembranes* **24**, 555–566.

Sprott GD, Ekiel I, Dicaire C (1990) Novel, acid-labile, hydroxydiether lipid cores in methanogenic bacteria. *Journal of Biological Chemistry* **265**, 13735–13740.

Sprott GD, Dicaire CJ, Choquet CG, Patel GB, Ekiel I (1993) Hydroxyether lipid structures in *Methanosarcina* spp. and *Methanococcus voltae*. *Applied and Environmental Microbiology* **59**, 912–914.

Stadniskaia A, Baas M, Ivanov MK, van Weering TCE, Sinninghe Damsté JS (2003) Novel archaeal macrocyclic diether core membrane lipids in a methane-derived carbonate crust from a mud volcano in the Sorokin Trough, NE Black Sea. *Archaea* **1**, 165–173.

Stadnitskaia A, Muyzera G, Abbas B, Coolena MJL, Hopmans EC, Baas M, van Weering TCE, Ivanov MK, Poludetkina E, Sinninghe Damsté JS (2005) Biomarker and 16S rDNA evidence for anaerobic oxidation of methane and related carbonate precipitation in deep-sea mud volcanoes of the Sorokin Trough, Black Sea. *Marine Geology* **217**, 67–96.

Stadnitskaia A, Bouloubassi I, Elvert M, Hinrichs K-U, Sinninghe Damsté JS (2008) Extended hydroxyarchaeol, a novel lipid biomarker for anaerobic methanotrophy in cold seepage habitats. *Organic Geochemistry* **39**, 1007–1014.

Stewart PS (2003) Diffusion in biofilms. *Journal of Bacteriology* **185**, 1485–1491.

Stiehl T, Rullkötter J, Nissenbaum A (2005) Molecular and isotopic characterization of lipids in cultured halophilic microorganisms from the Dead Sea and comparison with the sediment record of this hypersaline lake. *Organic Geochemistry* **36**, 1242–1251.

Stoodley P, Sauer K, Davies DG, Csterton JW (2002) Biofilms as complex differentiated communities. *Annual Review of Microbiology* **56**, 187–209.

Sugai A, Uda I, Itoh YH, Itoh T (2004) The core lipid composition of the 17 strains of hyperthermophilic archaea, *Thermococcales*. *Journal of Oleo Science* **53**, 41–44.

Summons RE, Jahnke LL, Roksandic Z (1994) Carbon isotopic fractionation in lipids from methanotrophic bacteria: relevance for interpretation of the geochemical record of biomarkers. *Geochimica et Cosmochimica Acta* **58**, 2853–2863.

Takai K, Nakamura K, Toki T, Tsunogai U, Miyazaki M, Miyazaki J, Hirayama H, Nakagawa S, Nunoura T, Horikoshi K (2008) Cell proliferation at 122 °C and isotopically heavy CH4 production by a hyperthermophilic methanogen under high-pressure cultivation. *Proceedings of the National Academy of Sciences USA* **105**, 10949–10954.

Teixidor P, Grimalt JO (1992) Gas chromatographic determination of isoprenoid alkylglycerol diethers in archaebacterial cultures and environmental samples. *Journal of Chromatography* **607**, 253–259.

Thiel V, Peckmann J, Schmale O, Reitner J, Michaelis W (2001) A new straight-chain hydrocarbon biomarker associated with anaerobic methane cycling. *Organic Geochemistry* **32**, 1019–1023.

Tornabene TG, Langworthy TA, Holzer G, Oro J (1979) Squalenes, phytanes and other isoprenoids as major neutral lipids of methanogenic and thermoacidophilic "archaebacteria". *Journal of Molecular Evolution* **13**, 73–83.

Uda I, Sugai A, Itoh YH, Itoh T (2001) Variations on molecular species of polar lipids from *Thermoplasma acidophilum* depends on growth temperatures. *Lipids* **36**, 103–105.

Van de Vossenberg JLCM, Driessen AJM, Konings WN (1998) The essence of being extremophilic: the role of the unique archaeal membrane lipids. *Extremophiles* **2**, 163–170.

Wakeham S, Amann R, Freeman KH, Hopmans EC, Jørgensen BB, Putnam IF, Schouten S, Sinninghe Damsté JS, Talbot HM, Woebken D (2007) Microbial ecology of the stratified water column of the Black Sea as revealed by a comprehensive biomarker study. *Organic Geochemistry* **38**, 2070–2097.

Werne J, Baas M, Sinninghe Damsté JS (2002) Molecular isotopic tracing of carbon flow and trophic relationships in a methane-supported benthic microbial community. *Limnology and Oceanography* **47**, 1694–1701.

Werne JP, Sinninghe Damsté JS (2004) Mixed sources contribute to the molecular isotopic signature of methane-rich mud breccia sediments of Kazan mud volcano (eastern Mediterranean). *Organic Geochemistry* **36**, 13–27.